Porous Template Scaffolds as a Three-Dimensional Culture Platform for Mesenchymal Stem Cells

Taylor Watson

A thesis

submitted in partial fulfilment of the

requirements for the degree of

Master of Science in Bioengineering

University of Washington

2021

Committee:

James Bryers

Billanna Hwang

Program Authorized to Offer Degree:

Bioengineering

University of Washington

ABSTRACT

Porous Template Scaffolds as a Three-Dimensional Culture Platform for Mesenchymal Stem Cells

Taylor Watson

Chair of the Supervisory Committee:

James Bryers

Bioengineering

Mesenchymal stem cells (**MSCs**) have been investigated for therapeutic applications due to their regenerative and immunomodulatory properties. While the cells show promise for eventual clinical translation, barriers remain that restrict their use. Traditional two-dimensional culture limits MSCs' sustained culture as they exhibit decreased paracrine and differentiation potential over time. Additionally, MSCs as a cellular therapy pose a risk to patients as they have been observed to differentiate into tumor and fibrotic cells. Three-dimensional culture of MSCs has been explored to mitigate the limits of two-dimensional culture while utilizing MSCs' secreted materials, especially exosomes, which have been explored as a lower risk cell-free therapy. Porous precision-templated scaffolds (**PTS**) are three-dimensional biomaterial constructs in which pore size and pore interconnects are precisely tunable and uniform in size throughout the

scaffold. Regardless of the polymer used in construction, PTS with uniform pores between 30 and 40 μm have shown enhanced healing characteristics by decreasing fibrosis and increasing the vascular host response. PTS were investigated as a potential three-dimensional culture platform for MSCs. MSCs within the scaffolds were imaged utilizing two-photon microscopy to evaluate if the cells were able to expand uniformly throughout the PTS. Additionally, MSCs cultured three-dimensionally were assessed relative to those grown two-dimensionally based on gene expression levels of the cells themselves as well as the effect the cells elicit in other cell lines, from both isolated exosomes and sustained paracrine exposure in coculture. When imaged within the scaffolds at 48 hour and 96 hour post-seeding, the MSCs were observed to migrate throughout the PTS, proliferating and forming pore-spanning connections with neighboring cells. Gene expression analysis via qPCR found overall increased expression of several inflammatory gene markers implicated in MSCs' paracrine effects in cells cultured three-dimensionally, relative to those cultured two-dimensionally. However, there was no clear difference in the polarization effect of exosomes isolated from MSCs cultured two- and three-dimensionally. The PTS scaffolds present as a promising three-dimensional culture platform for MSCs, warranting further investigation into their ability to preserve MSC differentiation potential as well as the ability to modify MSC phenotypes and the immunomodulatory properties of subsequently generated exosomes.

TABLE OF CONTENTS

LIST OF FIGURES

LIST OF TABLES

ACKNOWLEDGEMENTS

I would like to thank Dr. James Bryers for accepting me in his laboratory in my sophomore year and for serving as my principal investigator for the past 3 years. I've appreciated his feedback on my research as well as my writing. His guidance has helped shape my academic and professional development. I would also like to show gratitude to Dr. Billanna Hwang and Dr. Michael Mulligan for providing resources and advice that were instrumental to my research. I would like to especially thank Dr. Hwang for being in my committee and for providing her time and expertise to help guide my project. Her advice has helped me hone my technical and critical thinking skills and has overall made me a better researcher. Additionally, I would like to thank her for all of the snacks and lab meeting treats she provided over the years.

My work would not have been possible without all of the advice, training, and support I received from researchers in both the Bryers and Mulligan/Hwang labs, namely: Nathan Chan, Thomas Hady, Jen Merk, An Tran, and Rachel Waworuntu. From teaching me how to culture cells, to helping me navigate different laboratory equipment, to listening to me rant about video games; they all provided an informative and enjoyable laboratory environment that I'm very grateful to have been a part of.

Finally, I would like to thank my family for providing support throughout the entirety of my research. Thank you for every cup of coffee, every drive to Seattle, and every minute spent listening to me talk about my work, even when you had no idea what I was talking about.

CHAPTER 1. INTRODUCTION

1.1 Mesenchymal Stem Cells

Mesenchymal stem cells (**MSCs**) are adult-derived multipotent progenitor cells that are capable of self-renewal and differentiation into a variety of cell types, including osteocytes and adipocytes[1]. Because of their unique characteristics, MSCs have emerged as cells of interest for a variety of clinical applications, such as tissue repair and immunoregulation.

There are several factors that make MSCs promising candidates for tissue repair. One important characteristic is the variety of sources for stem cells[2]. MSCs have been isolated from a range of tissues, such as bone marrow, adipose tissue, umbilical cord blood, and synovium. This breadth of sources for MSCs both makes them readily available and tunable to the intended use, as MSCs sourced from different tissues exhibit different differentiation potential. For example, researchers have found that bone marrow-derived MSCs (BMSCs) exhibit increased osteogenic differentiation potential and decreased adipogenic differentiation potential in comparison to adipose tissue-derived MSCs (AMSCs)[3]. In addition to differentiation potential, tissue source has been found to influence MSC migration[4]. This variable migration pattern allows researchers to improve targeting of the tissue to be repaired based on the source of the MSCs. While regenerative medicine tends to utilize MSCs' homing and differentiation capabilities to repair damaged/disease tissue, there is another aspect of MSCs that makes them of clinical interest: their immunomodulatory capabilities.

MSCs have been found to regulate the immune response at several points and via several mechanisms[5]. MSCs can suppress T lymphocyte activation and proliferation both by direct cell-cell interactions and the release of soluble factors[6,7]. Similarly, MSCs inhibit B lymphocyte proliferation and dendritic cell function both when able to directly interact with the cells and when physically separated and only able to interact via their secretome[8]. Because of this robust and well-rounded immunomodulation, MSCs are of clinical interest for a variety of immune conditions. Clinical trials have been conducted on the use of MSCs to treat patients with graft-versus-host-disease, diabetes, and Crohn's disease, among other conditions[9]. Their immunoregulatory capabilities add to MSCs' use in regenerative medicine, as modulating the immune response is critical in the restoration of certain tissues, such as by inhibiting fibrosis to improve liver function[2]. Despite the range of benefits and capabilities of MSCs, there are still barriers to their translation for clinical use.

One of the biggest concerns for MSC-based therapies is safety. MSCs can differentiate into tumors, as studies have indicated that some cases of Ewing's sarcoma and glioma have been derived from MSCs and other stem cells[10,11]. Additionally, MSCs' immunomodulatory capabilities and pro-angiogenic functions can promote the growth and metastasis of already present tumor cells[12]. Beyond tumorigenicity, MSC-based treatments have a risk of promoting inflammation as their immunosuppressive capabilities have been demonstrated to require sufficient levels of proinflammatory cytokines[13]. Furthermore, MSCs may promote fibrosis by differentiating into myofibroblasts, impeding tissue repair[14]. Due to these potential risks, cell-free alternatives are being explored. One potential alternative seeks to avoid MSC-associated complications while maintaining MSC-associated benefits: MSC-derived exosomes.

1.2 Exosomes

Extracellular vesicles (**EVs**) are lipid bound vesicles secreted by a variety of cell types that carry biomolecular cargo, including proteins, lipids, RNA, and DNA[15]. One subset of extracellular vesicles is exosomes, which are characterized by their endosomal formation and their small size (30-150 nm in diameter, on average). Since exosomes and other EVs' cargoes are derived from and defined by their parent cells, they have been identified as important mediators of cell-cell communication[16]. Due to this important biological function, exosomes have emerged as a promising resource for varied clinical applications, including diagnostics as well as therapeutics.

Exosomes are secreted from cells under both healthy and diseased conditions, carrying biomolecules that reflect the state of their parent cells[17]. This biomolecular cargo can serve as biomarkers for diagnostics. Exosomal proteins have been identified as potential diagnostic tools in a variety of diseases, such as EGFRvIII, a tumor-specific antigen that has been observed in exosomes from patients with glioblastoma multiforme[18]. In a similar manner, exosomal nucleic acids have been found to vary under different pathologies, allowing these nucleic acids to be used as biomarkers. For example, exosomes isolated from the urine of patients with chronic kidney disease were found to have varying levels of miRNA-29 based on the patient's degree of renal fibrosis, identifying this miRNA as a potential noninvasive marker for kidney disease and fibrosis[19]. Beyond carrying cargo derived from parent cells that may act as biomarkers, exosomes have also been implicated in contributing to different pathologies. One disease found to utilize the cell-cell communication provided by exosomes is cancer[20]. Tumor cells employ exosomes to both protect themselves and impact surrounding cells. For self-preservation, both

cancerous and healthy cells secrete exosomes to maintain homeostasis and expel cytoplasmic DNA[21]. When exosome secretion is suppressed, this cytoplasmic DNA has been observed to accumulate and lead to apoptosis. Tumor cells can also prevent apoptosis in surrounding cells via exosomal transfer of cytokines that block apoptotic pathways, such as TGF-β1, contributing to tumor survival and growth[22]. To further promote tumor growth and metastasis, cancerous cells can transfer oncogenic proteins, such as mutated KRAS and splicing factors, to surrounding cells, increasing proliferation and, in some cases, therapy-resistance[23,24]. As much as diseases can exploit the communication capabilities of exosomes, researchers can exploit those same capabilities to develop therapeutics.

Exosomes have several unique characteristics that identify them as promising therapeutic candidates for a variety of diseases. Since exosomes are biologically derived, they offer low immunogenicity, high stability in the body, and a capacity to cross the blood-brain barrier[25]. Another important benefit of exosomes is their capacity to be loaded with therapeutic cargo[26]. Since exosomes contain biomolecules derived from their parent cells, one way to engineer exosomes is by directly modifying their cellular source. For example, researchers have found that transfecting parent cells with an anti-tumor miRNA results in secreted exosomes that contain the miRNA and are able to reduce tumor xenograft growth upon exosome injection[27]. Alternatively, exogenous cargo can be directly loaded into isolated exosomes via a variety of methods to fuse with or disrupt the lipid bilayer, such as lipofection and electroporation[26]. Beyond internal cargo, exosome surfaces can also be engineered post-isolation. By modifying the surface of exosomes, their therapeutic use is improved and expanded. Exosomal surfaces can be functionalized to include targeting molecules, reducing the risk of off target effects[28].

Additionally, the surfaces can be functionalized optically with fluorescent or bioluminescent molecules, presenting imaging as a potential application of exosomes. However, exosomes can also be utilized without engineering as they possess beneficial characteristics of their parent cells. Because of this, MSC-derived exosomes have emerged as a promising cell-free alternative to MSC-based therapeutics.

MSC-derived exosomes mirror the therapeutic characteristics of their parent cells and serve as mediators for MSCs' paracrine effects[29]. These vesicles have been observed to suppress the immune response and prevent damaging inflammation in different pathologies in a similar manner to MSCs[30-32]. In addition to MSCs' immunomodulatory capabilities, their exosomes also promote proliferation and reduce fibrosis, making them similarly fit for regenerative medicine applications[33,34]. Several preclinical studies have been conducted on the effects of MSC-derived exosomes on a variety of diseases, with neurological, cardiovascular, and immunological diseases being the most prevalent[35]. While utilizing exosomes as an alternative therapeutic source avoids the potential cell-based risks of MSC therapies, they also share some of the other challenges found in translating MSC therapies to a clinical setting. One of the largest challenges in MSC-exosome translation is the decrease in their differentiation potential and surface protein expression with sustained expansion in two-dimensional culture[36]. To mitigate these deleterious effects of sustained two-dimensional culture, researchers have explore growing MSCs in three-dimensional cultures.

1.3 Three-Dimensional Culture of Mesenchymal Stem Cells

Due to the limited differentiation and paracrine capacities of MSCs in sustained two-dimensional culture, three-dimensional culture platforms have been explored to maintain the cells' multipotency and paracrine activity. It is thought that these three-dimensional cultures are better able to reflect the *in vivo* MSC environment, as the cells are able to proliferate in more dimensions as well as form more complex cell-cell interactions and extracellular matrix (ECM) structures[37].

The comparison of two-dimensional and three-dimensional cultures of MSCs has yielded data that suggests three-dimensional cultures not only improve the survival of MSCs *in vitro*, but also sustain their therapeutic properties. MSCs grown in spheroids have been found to exhibit increased expression of pluripotent markers, such as SOX2 and OCT4, relative to those grown in two-dimensional cultures[38,39]. This upregulated expression of proliferation-associated genes reflects the increased differentiation capacities of MSCs grown three-dimensionally. Similar levels of increased multipotency were seen with MSCs cultured in hydrogels, suggesting that increased differentiation capacity can be attributed to the shared three-dimensional nature of these culture platforms, as opposed to different characteristics unique to the individual types of culture[40]. The increased expression of multipotency markers indicates that MSCs can be cultured three-dimensionally for longer periods of time than two-dimensionally while retaining their stemness and self-renewing properties. Longer sustained culture with maintained therapeutic properties is required for improved scaling of MSC culture for eventual clinical translation of MSC-based therapeutics.

Beyond multipotency, three-dimensional cultures of MSCs have been shown to exhibit improved differentiation into different cell types. In scaffold based culture, MSCs have been shown to exhibit increased hepatic differentiation when stimulated with valproic acid relative to MSCs grown two-dimensionally[41]. In spheroid cultures, MSCs have exhibited increased osteogenic and adipogenic differentiation[39,42]. These improved differentiation capabilities are of interest for applications of MSCs in regenerative medicine where the goal is to replace/rebuild the damaged tissue.

Due to the observed beneficial effects of three-dimensional culture on MSC expansion and therapeutic potential, several platforms for three-dimensional culture have been developed and explored. Spheroid cultures are formed as MSCs self-assemble into aggregated clusters[38]. While these clusters allow the contained MSCs to form more complex cell-cell and cell-matrix interactions, there is the risk of the cells in the core developing hypoxia or necrosis[43]. An alternative platform that has been explored is hydrogel-based culture. Hydrogel cultures are able to mimic the *in vivo* environment of MSCs due to their tunable structural properties that can be designed to emulate soft tissue[44]. However, similar to spheroid-based cultures, there are limitations on hydrogel culture size as nutrients may not be able to diffuse throughout the entire hydrogel, inhibiting the growth and survival of those MSCs further from the nutrient source. One culture platform that better allows for the diffusion of nutrients throughout the culture is scaffold-based cultures. Scaffolds designed for cellular culture are porous, facilitating nutrient access to all cells within the culture[45]. Additionally, scaffold structures and mechanical properties can be tuned, much like hydrogels, to achieve different MSC expression profiles and differentiation capabilities[46-48]. One type of scaffold with tunable and replicable capabilities that

makes them of interest for three-dimensional MSC culture is porous precision-templated scaffolds.

1.4 Porous Precision-Templated Scaffolds

Porous precision-templated scaffolds (**PTS**) have been developed by the Ratner group and utilized for tissue regeneration by groups such as the Bryers and Mulligan labs[49-51]. PTS scaffolds are created using a patented sphere-templating method that allows for control over uniform pore and pore-interconnect size[52]. The ability to precisely control the structure of the scaffolds is important as these varying structural properties have been observed to elicit different reactions from cells based on pore and interconnect size. One study found that PTS scaffolds with 30-40 μm diameter pores exhibited increased angiogenesis and reduced fibrosis relative to 100 μm pore scaffolds when implanted in the myocardium of rats[53]. This reduction in inflammation is reflective of a more pro-healing effect and coincides with increased M2 polarization in resident macrophages, the macrophage phenotype associated with immunomodulatory and wound healing functions. Similar differences between 40 and 100 μm pore scaffolds were observed in experiments investigating the impact of pore size on dendritic cell (**DC**) maturation and activation[54]. In this study, PTS scaffolds with smaller pores were observed to increase DC maturation *in vitro* and increase DC recruitment/activation *in vivo* when implanted subcutaneously in mice. These findings further illustrate the ability of PTS scaffolds' structural properties alone to influence the behavior of resident cells. Since the pore and interconnect size of PTS can influence the behavior and expression of their resident cells, these structural properties can potentially influence the exosomes secreted by these cells. When

comparing the exosomes generated by cells inhabiting 40 and 100 μm PTS after subcutaneous implantation in mice, it was found that those exosomes isolated from implanted 100 μm scaffolds induced inflammatory gene expression in T cells[51]. Conversely, exosomes derived from cells inhabiting 40 μm PTS exhibited a more immunomodulatory effect, which would be preferable for wound healing and other regenerative therapeutic applications. Since PTS have demonstrated such control over the expression and polarization of their contained cells, these scaffolds are of interest for MSC culture.

1.5 Introduction to Thesis Work

The objective of this thesis is to investigate the potential use of PTS scaffolds as a three-dimensional culture platform for MSCs.

The two specific aims of this project are as follows:

Aim 1. Develop the methods to quantify and non-invasively characterize *in vitro* the inoculation, cell spreading, and cell migration of MSCs in PTS.

Aim 2. Quantify MSCs *in vitro* cultivated both two-dimensionally and in three-dimensional PTS. Characterize the paracrine capabilities of and EVs generated in traditional *in vitro* two-dimensional MSC cultures compared to those of MSCs cultivated in 40 and 100 μm PTS.

CHAPTER 2. METHODS

2.1 Culture of Mesenchymal Stem Cells in Porous Template Scaffolds

Porous template scaffolds with 40 and 100 µm pores were fabricated using the sphere-templating method generated by the Ratner group and currently in use in the Bryers lab[49,52]. Poly (methyl methacrylate) (PMMA) beads (40µm and 100µm OD) were obtained from Microbeads AS (Skedsmokorset, Norway). A mold was created by placing 1 mm thick Teflon strips (2 mm wide) to serve as a retaining gasket between two 75 mm x 25 mm x 1 mm glass slides. Beads of the desired pore size were poured into the cavity. Molds filled with beads were placed in a water bath sonicator for 2 hours to ensure uniform packing. Beads were then sintered to each other at their contacts points by heating at 175°C (40µm) or 179°C (100µm) for 24 hrs. The sintering procedure was optimized to obtain PMMA templates with neck sizes (interconnects between the beads) that were approximately 30% of the bead diameter. Poly(hydroxyethyl methyacrylate) (**pHEMA**) was selected over other polymers for its superior performance in histology dissection, biological inertness, and stability. pHEMA precursor consisted of 5 mL 2-hydroxyethyl methacrylate (HEMA) (Polysciences, ophthalmic grade), 0.23 mL tetraethyleneglycol dimethacrylate (TEGDMA) (Polysciences), 2.0 mL deionized water, 3.6 mL ethylene glycol, and 20 mg 2, 2-dimethoxy-2-phenylacetophenone (Irgacure 651) (BASF, Freeport, LA). The reaction mixture was infiltrated into the glass mold surrounding the bead template and degassed under vacuum for 30 minutes. HEMA monomer was free-radical polymerized to pHEMA under a 450W broad-spectrum UV lamp for 15 minutes. After polymerization, the PMMA bead template

surrounded by the polymerized pHEMA was removed from the mold and placed in acetone to dissolve the PMMA microspheres. The resulting porous scaffolds, composed of pHEMA, were cut into 5 mm discs using a biopsy punch.

The MSCs were isolated from clones in use by the Mulligan/Hwang lab, specifically clone O and clone N^{55}. The cells were harvested from Nunc™ EasYFlask™ 75 cm^2 Cell Culture Flasks when they were 90-95% confluent. This was done by first aspirating the medium before adding 3 mL of Thermo Fisher Trypsin-EDTA (0.25%), phenol red to remove the adherent MSCs from the flask surface. The trypsin was left on the cells for 2 minutes before the resulting cell suspension was removed and added to Falcon™ 15 mL Conical Centrifuge Tubes. An equal volume of medium (Thermo Fisher RPMI 1640 medium with 10% FBS and 1% Pen-Strep) was added to the tubes to neutralize the trypsin and prevent toxicity to the cells. The suspension was then spun at 1000 RPM for 10 minutes to pellet the cells. The supernatant was then removed from the tube, and the pellet resuspended in 1 mL of medium.

Once isolated, the MSCs were seeded within the PTS scaffolds. To infiltrate the scaffolds with the cells, scaffolds were placed upon sterilized Kimtech™ Science Kimwipes. Cellular suspensions of 500,000 MSCs were pipetted onto each scaffold. Due to the fibrous nature of the Kimwipes, capillary action pulled the suspensions through the scaffold. The seeded scaffolds were then placed in 6-well plates with one scaffold and 2 mL of medium per well. These plates were incubated and allowed to expand for 48 hours.

2.2 Multi-Photon Imaging of Mesenchymal Stem Cells in Scaffold Cultures

To visualize and quantify the growth of MSCs within the PTS scaffolds, clone O MSCs were seeded and expanded within the scaffolds as described above. Prior to seeding, these MSCs were stained with carboxyfluorescein succinimidyl ester (CFSE), in accordance with the protocol provided in the CellTrace™ CFSE Cell Proliferation Kit[56]. Cell-laden scaffolds were allowed to incubate for 0, 24, and 48 hours. Due to the dilution of CFSE fluorescence as cells divide and proliferate, a set of cell-laden scaffolds at a later timepoint were stained with NucBlue™ in addition to CFSE, in accordance with the manufacturer's protocol[57]. These cells were allowed to incubate for 0, 24, 48, 72, and 96 hours. After incubation, the cells were fixed within the PTS by submerging the PTS in 2 mL of 10% formalin for 10 minutes. Following fixation, the scaffolds were optically "cleared" (matching the optical refractive index of the pHEMA) by being submerged in benzyl alcohol for 3 hours until rendered transparent. Once transparent, the PTS were mounted on 75 mm x 38 mm glass microscope slides. Each PTS was covered in Omnimount, a transparent mounting fixative with low inherent fluorescence. A glass coverslip was then placed atop each scaffold, with additional Omnimount infiltrated below the coverslip to ensure the PTS were completely surrounded by the mounting agent, preventing drying of the scaffold. Small weights were placed atop of the coverslips to keep the surface flat. The mounted slides were placed within a convection oven for 2 hours before being allowed to dry for 7 days.

PTS were imaged using the Olympus FV1000 Multi-photon microscope (Lynn and Mike Garvey Imaging Core at the University of Washington's SLU campus). An excitation wavelength of 780

nm was utilized. CFSE has an emission wavelength of 520 nm, requiring the FV10-MRV/G filter cube for violet and green light[56,58]. NucBlue™ has an emission wavelength of 460 nm, falling within the spectra of the FV10-MRV/G filter cube[57]. A droplet of water was placed on the coverslip above each scaffold to allow for an Olympus 10x 0.6 NA water immersion objective to obtain the images. With Olympus' multi-photon microscope software, Fluoview FV1000, mosaic imaging was conducted to optically section each scaffold entirely. In mosaic imaging, the boundaries of the sample are outlined and the microscope's motorized XY stage is programmed to move the sample, capturing multiple images that may be stitched together to form an image of the entire sample. Additionally, XYZ acquisition was utilized to image the scaffolds three-dimensionally. The individual Z-stacks were stitched together utilizing XuvStitch[59]. Imaris was used to reconstruct these stitched Z-stacks to create a three-dimensional image. To improve the clarity of these images, noise reduction filters within Imaris were used. To quantify the data of the imaged scaffolds, the processed three-dimensional images were analyzed with ImageJ using Bob Dougherty's Measure Stack plugin[60].

2.3 Mesenchymal Stem Cell Two- and Three-Dimensional Cultures

To compare the effect of two- and three-dimensional culture conditions on MSCs and their generated exosomes, MSCs were simultaneously cultured within tissue culture plates and PTS. Clone O and N MSCs were individually seeded within both 40 and 100 μm PTS and placed within 6-well plates with 2 mL of medium at a concentration of 500,000 cells per scaffold. Additionally, clone O and N MSCs were cultured within the wells of the 6-well plate two-dimensionally at a concentration of 50,000 cells per well. Different seeding concentrations were

chosen to maintain percent confluency between the two-dimensional wells and the PTS with increased surface area. After 24 and 48 hours, the cells and medium from the two- and three-dimensional cultures were isolated. These timepoints were selected to maintain the timescale established in the PTS imaging experiments. Medium was transferred from the wells to 15 mL conical tubes for short term storage at -20 ºC prior to exosome isolation. From the two-dimensional cultures, cells were isolated by applying 2 mL of trypsin to the wells to detach the MSCs from the surface. After detachment, the trypsin and cells were transferred to a 15 mL conical tube with 2 mL of medium to halt trypsin activity before being centrifuged at 1000 RPM for 10 minutes, pelleting the MSCs. From the three-dimensional cultures, PTS were cut into 4 pieces and placed into 2 mL of fresh medium in a 6-well plate to allow the MSCs to leach out. The medium and cells were then transferred into a 15 mL conical tube to be centrifuged at 1000 RPM for 10 minutes, pelleting the MSCs. The pellets were stored at -20 ºC short term prior to RNA isolation. This process was conducted twice to increase sample size.

2.4 Treatment of RAW 264.7 Cells with Exosomes from Mesenchymal Stem Cells Cultured Two- and Three-Dimensionally

Exosomes were isolated from the isolated medium of the two- and three-dimensional MSC cultures using the Invitrogen™ Total Exosome Isolation Kit, according to the manufacturer's protocol. For each individual well/culture, 1 mL of medium (Thermo Fisher DMEM medium with 10% FBS and 1% Pen-Strep) was utilized to isolate exosomes and the resulting exosome pellets were resuspended in 200 µL of PBS. Macrophage-like RAW 264.7 cells were plated in 2 6-well plates at a concentration of 100,000 cells/well. Each well was treated with 150 µL of the

isolated exosomes and allowed to expand for 48 hours. The RAW 264.7 cells were harvested as described above for the two-dimensionally cultured MSCs. The 48 hour timepoint was selected to maintain the timescale utilized in the initial MSC culture. As with the MSC culture, this process was conducted twice to increase sample size.

2.5 Coculture of RAW 264.7 Cells with Mesenchymal Stem Cells Two- and Three-Dimensionally

To compare the impact of two- and three-dimensional culture on MSCs' paracrine effects on other cells, clone O and N MSCs were cocultured with RAW 264.7 cells utilizing Corning™ Transwell™ 6-well plate inserts with 0.4 μm pore size in accordance with the product's official protocol[61]. RAW 264.7 cells were seeded at a concentration of 50,000 cells/well in a 6-well plate while clone O and N MSCs were cultured within the well inserts. For the two-dimensional cultures, the MSCs were seeded at a concentration of 50,000 cells/insert. For the three-dimensional cultures, the MSCs were seeded at a concentration of 250,000 cells/scaffold. This lower scaffold seeding concentration was selected due to the increased timepoint. The cells were all cultured in Thermo Fisher RPMI 1640 medium with 10% FBS and 1% Pen-Strep and allowed to expand for 48 and 96 hours before being harvested as previously described. As with the previous cultures, this process was conducted twice to increase sample size.

2.6 Gene Expression Analysis of Mesenchymal Stem Cells From Two- and Three-Dimensional Cultures

RNA was extracted from the MSCs from the two- and three-dimensional cultures using the Qiagen RNeasy® Kit, according to the manufacturer's protocol. After isolation, the RNA from the MSCs was utilized to synthesize cDNA using the Applied Biosystems™ High-Capacity RNA-to-cDNA™ Kit, according to the manufacturer's protocol. After the MSC cDNA was synthesized, it was quantified with the Qubit™ ssDNA Assay Kit and Qubit™ Fluorometer, according to the manufacturer's protocol. qPCR was performed with SYBR green, including a panel of PPIA, IL-6, IL-10, iNOS, TGFβ1, and VEGFA probes on an ABI 7900HT Sequence Detection System. The rationale for this panel can be seen in Table 1. For each sample, two wells were analyzed per probe to provide duplicates. Expression was quantified by normalizing against peptidylprolyl isomerase A (**PPIA**), a housekeeping gene, (ΔCt), averaging the expression level between duplicate wells (Av. ΔCt), and expressing this average as a negative exponential ($2^{-Av.\ \Delta Ct}$).

Probe	Selection Rationale
IL-6	A pleiotropic cytokine involved in both pro- and anti-inflammatory signaling. Secreted by MSCs and found to impact their paracrine activity and proliferation[62].
IL-10	An anti-inflammatory cytokine. Secreted by MSCs and implemented in their protective effect on organs and regulation of immune cells[63,64].
iNOS	An inducible enzyme that catalyzes the oxidation of L-arginine and produces nitric oxide. Found to play a critical role in regulating autoimmune conditions and MSCs' therapeutic effects[65,66].
TGFβ1	A cytokine that controls cellular growth, differentiation, and proliferation. Secreted by MSCs and observed to impact their immunomodulatory and pro-healing effects[67,68].
VEGFA	A growth factor protein critical in angiogenesis. Secreted by MSCs and found to influence the differentiation of endothelial progenitor cells and promote vascularization in wound healing[69,70].

Table 1: *Rationale for the selection of genetic probes for the qPCR SYBR panel carried out on two- and three-dimensionally cultured MSCs.*

2.7 Gene Expression Analysis of RAW 264.7 Cells Treated with Exosomes Generated from MSCs in Two- and Three-Dimensional Cultures

After the 48-hour incubation, the RAW 264.7 cells were isolated using the aforementioned two-dimensional MSC isolation protocol. RNA isolation, cDNA synthesis, and cDNA quantification were performed utilizing the same kits as in the MSC qPCR preparation. qPCR was performed with SYBR green utilizing the aforementioned sequence detection system. In the RAW 264.7 cell qPCR, a macrophage panel was utilized that consists of PPIA, ARG-1, CD32, CD86,

CD206, FIZZ-1, IL1β, IL-6, IL-10, iNOS, TGFβ1, and YM1. Gene expression was quantified in the same format as the MSC qPCR, again with PPIA as a housekeeping gene.

2.8 Gene Expression Analysis of RAW 264.7 Cells and Mesenchymal Stem Cells Cocultured Two- and Three-Dimensionally

After the 48 and 96 hour incubation, the RAW 264.7 cells and MSCs were isolated using the aforementioned cell isolation protocols. RNA isolation, cDNA synthesis, and cDNA quantification were performed utilizing the same kits as previously mentioned. qPCR was performed with SYBR green utilizing the aforementioned sequence detection system. In the respective RAW 264.7 cell and MSC qPCRs, the previously described panels were retained. Expression was quantified in the same format as previously utilized, again with PPIA as a housekeeping gene.

CHAPTER 3. RESULTS AND DISCUSSION

3.1 Multi-Photon Microscopy of Mesenchymal Stem Cell Growth in Porous Template Scaffolds

Multi-photon microscopic optical section mosaics of the 40 μm PTS scaffolds seeded with CFSE stained clone O MSCs at the 0, 24, and 48 hour timepoints are shown, respectively, in Figures 1-3. Between the 0 and 24 hour timepoints, there is a decrease in the quantity of cells that suggests a significant amount of cells leach out into the medium during the initial incubation period. This was expected as the pHEMA used to fabricate the PTS isn't inherently adhesive for mammalian cells and MSCs are an adhesive cell line. However, there is an increase in the quantity of cells between the 24 and 48 hour timepoints that suggests the MSCs are capable of growing and expanding within the PTS scaffolds. This indicates that despite the cells not fully adhering during initial incubation, enough cells are able to adhere to either the scaffold or each other to expand within the PTS scaffold.

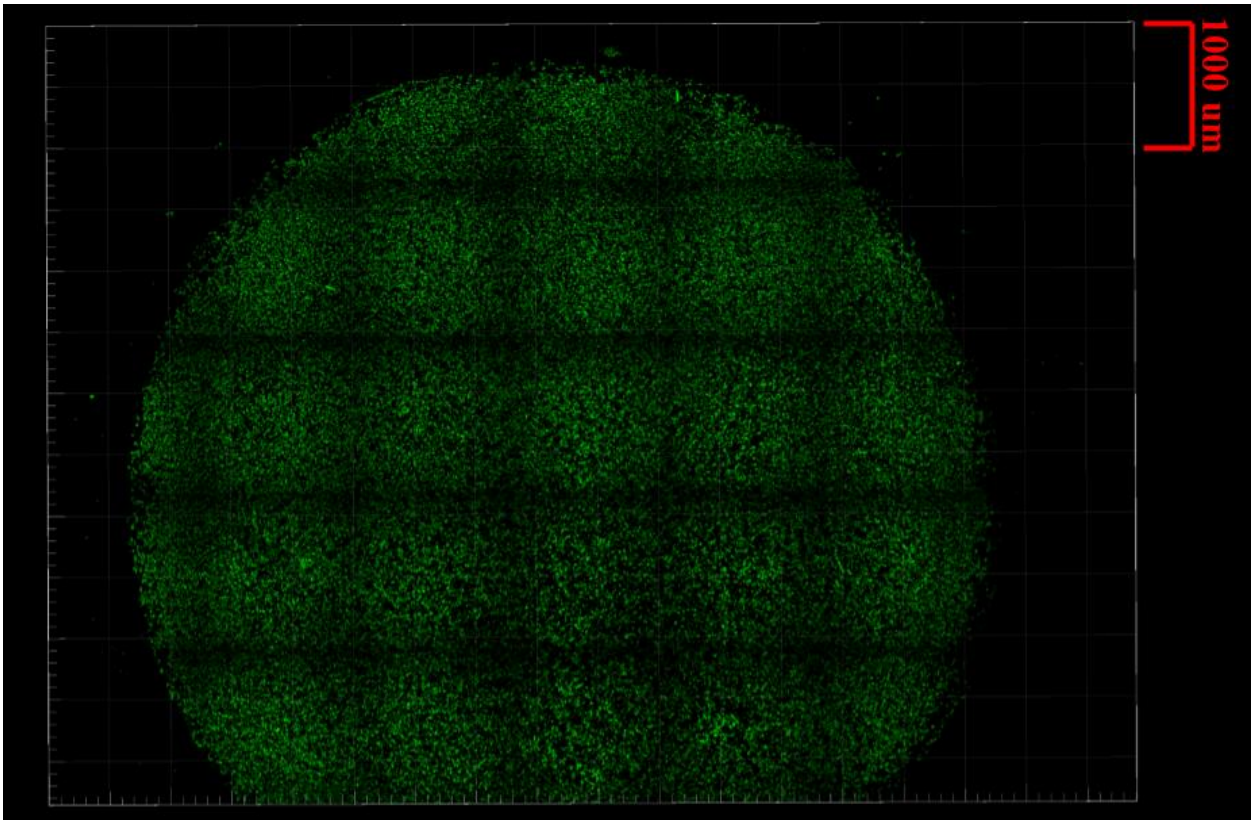

Figure 1: *A mosaic image of a 40 µm scaffold seeded with clone O MSCs at the 0 hour timepoint.*

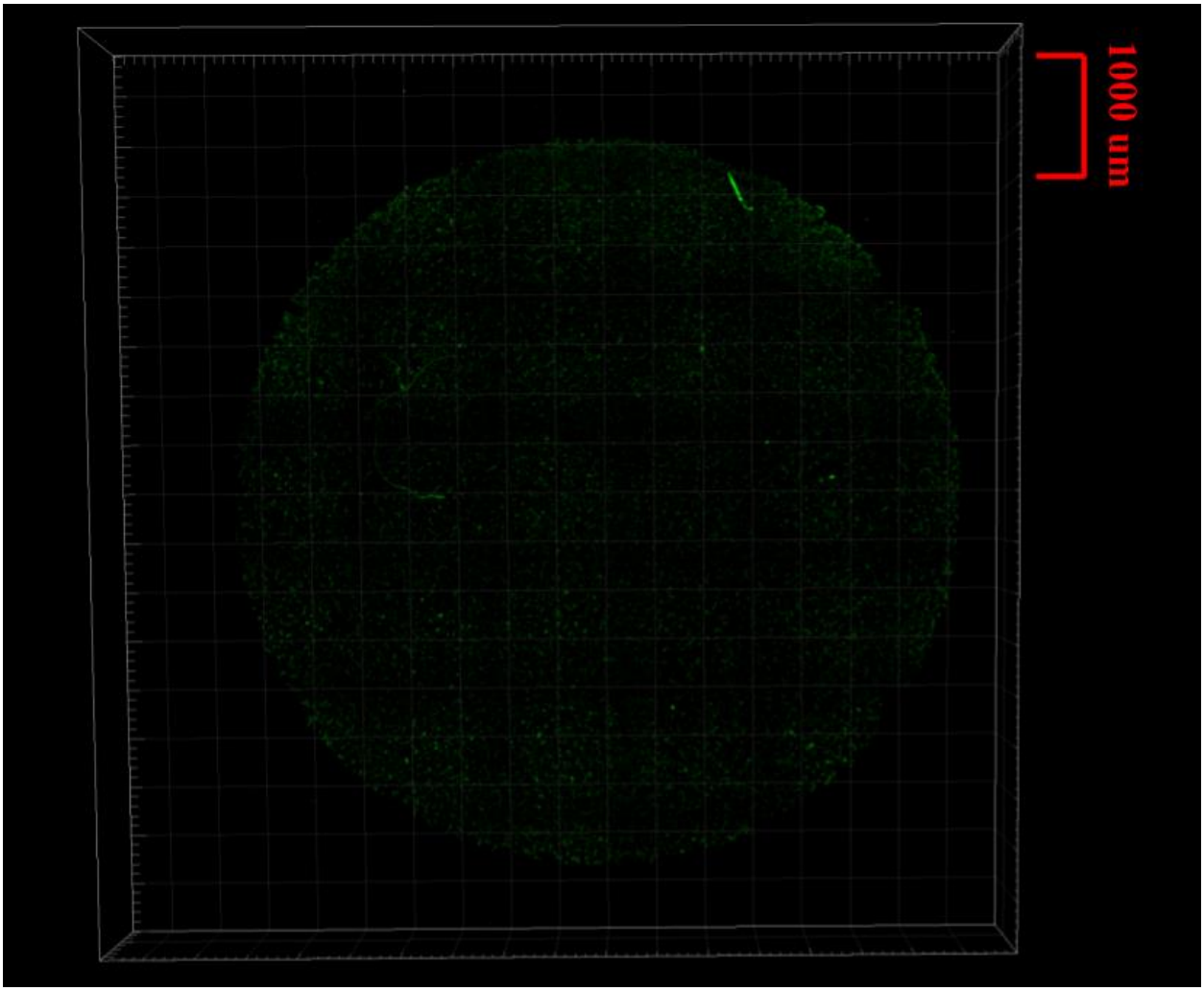

Figure 2: *A mosaic image of a 40 µm scaffold seeded with clone O MSCs at the 24 hour timepoint.*

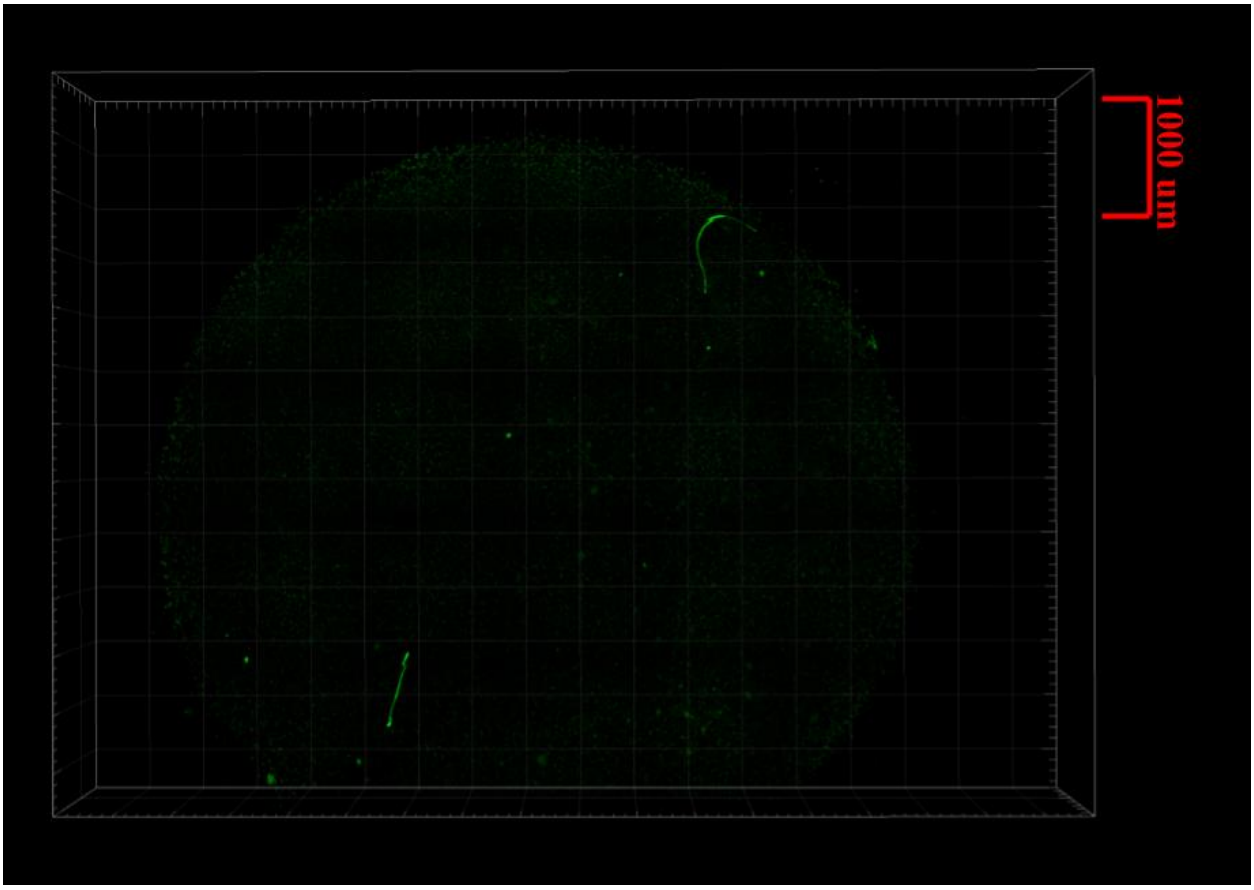

Figure 3: *A mosaic image of a 40 µm scaffold seeded with clone O MSCs at the 48 hour timepoint.*

After stitching the z-stacks of the imaged scaffolds together to fully visualize the complete volume, the mosaics were processed and analyzed with ImageJ[60]. Image processing allowed the quantification of MSC presence and growth within the scaffold, as summarized in Table 2. Within 24 hours, over 90% of cells leach out of the scaffold. Within another 24 hours (for 48 hours total incubation), the remaining cells grow, multiply, and divide and nearly completely recuperate the amount lost during the initial incubation phase, with over 90% of initial cells present.

Timepoint (hr)	Total Fluorescence	Volume of Scaffold Imaged (mm^3)	Fluorescence/Volume ($1/mm^3$)
0	4.89×10^7	30.344	1.61×10^6
24	1.69×10^6	34.408	4.91×10^4
48	4.54×10^7	29.416	1.54×10^6

Table 2: *Statistics of the MSCs within the imaged scaffolds obtained via ImageJ[60]. Total fluorescence refers to the data intensity sum, as measured with ImageJ. There is a decrease in fluorescence from the 0- to 24-hour timepoint, reflective of cells leaching out into the medium. This decrease in fluorescence is recuperated by the 48-hour timepoint, reflective of the MSCs expanding within the scaffold between the 24- and 48- hour timepoints.*

The significant loss of cells within the first 24 hours of culture is surprising, despite the limited adhesion of mammalian cells within pHEMA. Similarly, the recuperation of the cell loss within the next 24 hours reflects a surprisingly significant growth. This calls into question if the 24 hour timepoint was seeded with less cells initially or was otherwise compromised, reducing the cell content of the PTS scaffold. However, observing the similar fluorescence levels of MSCs within the 0 and 48 hour timepoints does indicate growth of the MSCs within the scaffolds as MSCs were observed to leach out of the PTS scaffold and seen within the 6-well plate the scaffold was placed in. The fact that that there are comparable quantities of MSCs within the 0 and 48 hour timepoint scaffold despite this cell loss does suggests that the MSCs are capable of expanding within the scaffolds, facilitating this recuperation.

To better characterize the growth of MSCs within PTS cultures over a longer time period, scaffolds laden with CFSE and NucBlue™ were imaged at 24 hour timepoints over 96 hours. These images can be seen in Figures 4-8. As with the previous experiments, cell loss was

observed between the 0 and 24 hour timepoints and cell growth was observed in the subsequent timepoints. These observations further support that MSCs are capable of adhering to and proliferating within the pHEMA scaffolds.

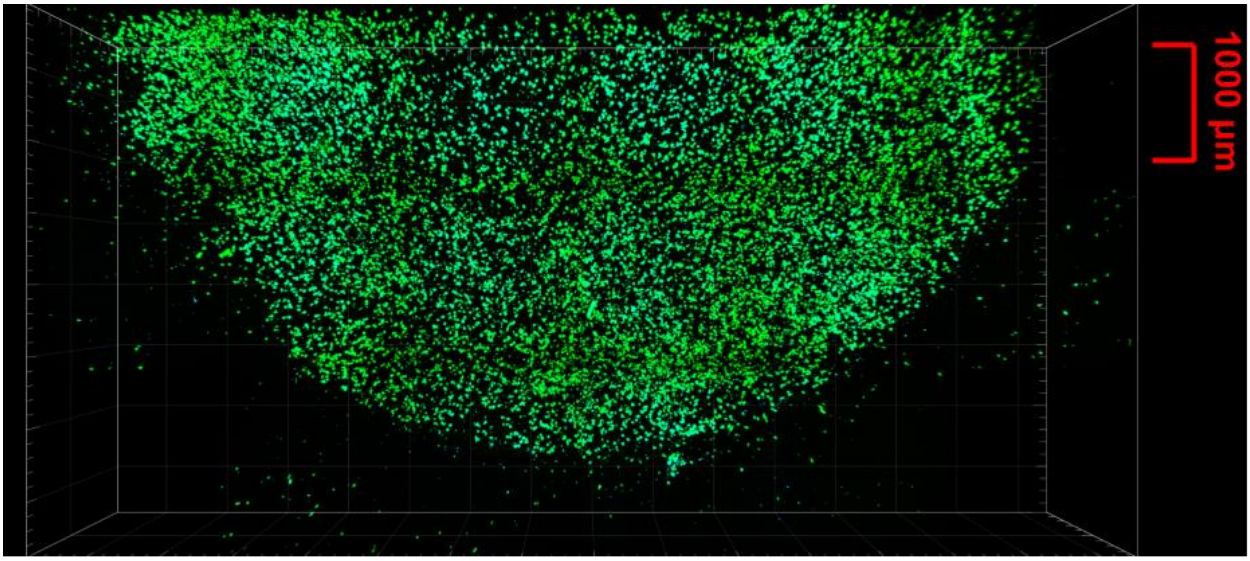

Figure 4: *A mosaic image of a 40 µm scaffold seeded with clone O MSCs stained with CFSE and NucBlue™ at the 0 hour timepoint.*

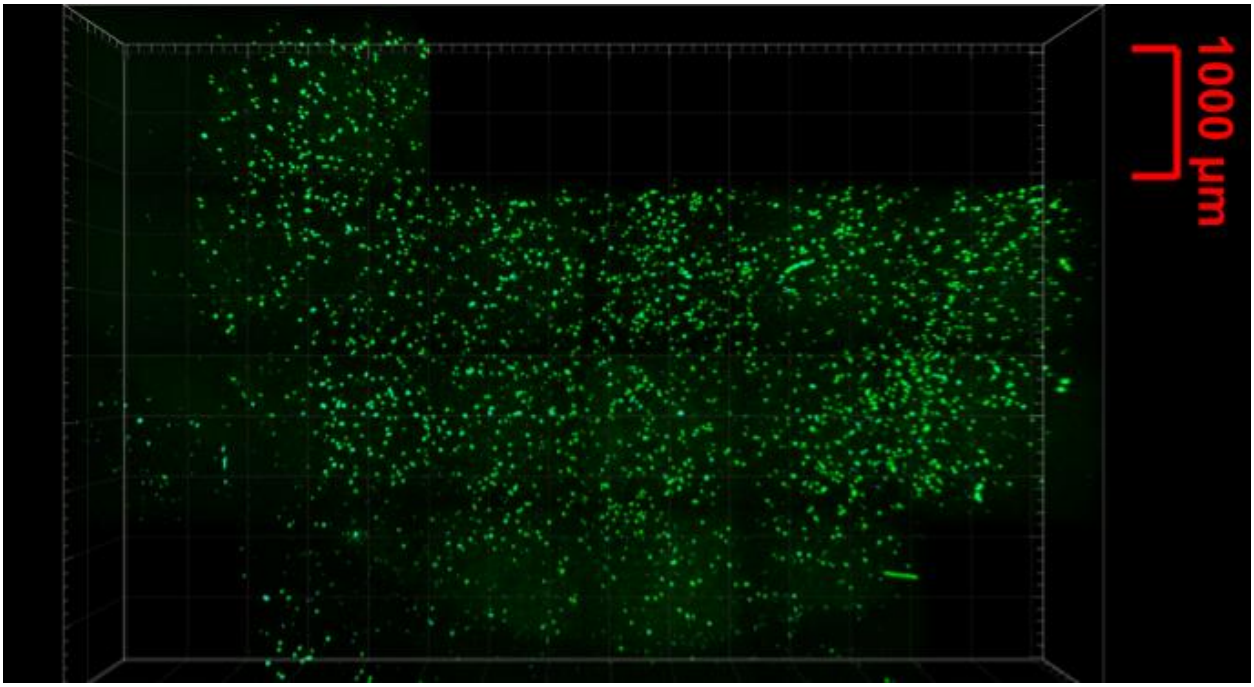

Figure 5: *A mosaic image of a 40 µm scaffold seeded with clone O MSCs stained with CFSE and NucBlue™ at the 24 hour timepoint.*

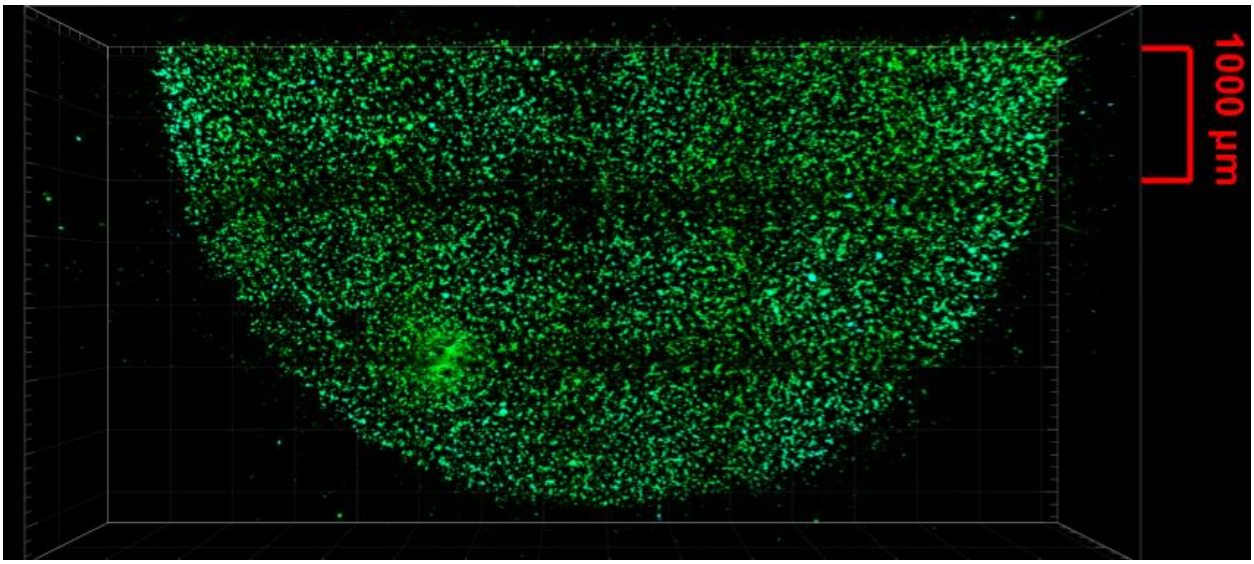

Figure 6: *A mosaic image of a 40 µm scaffold seeded with clone O MSCs stained with CFSE and NucBlue™ at the 48 hour timepoint.*

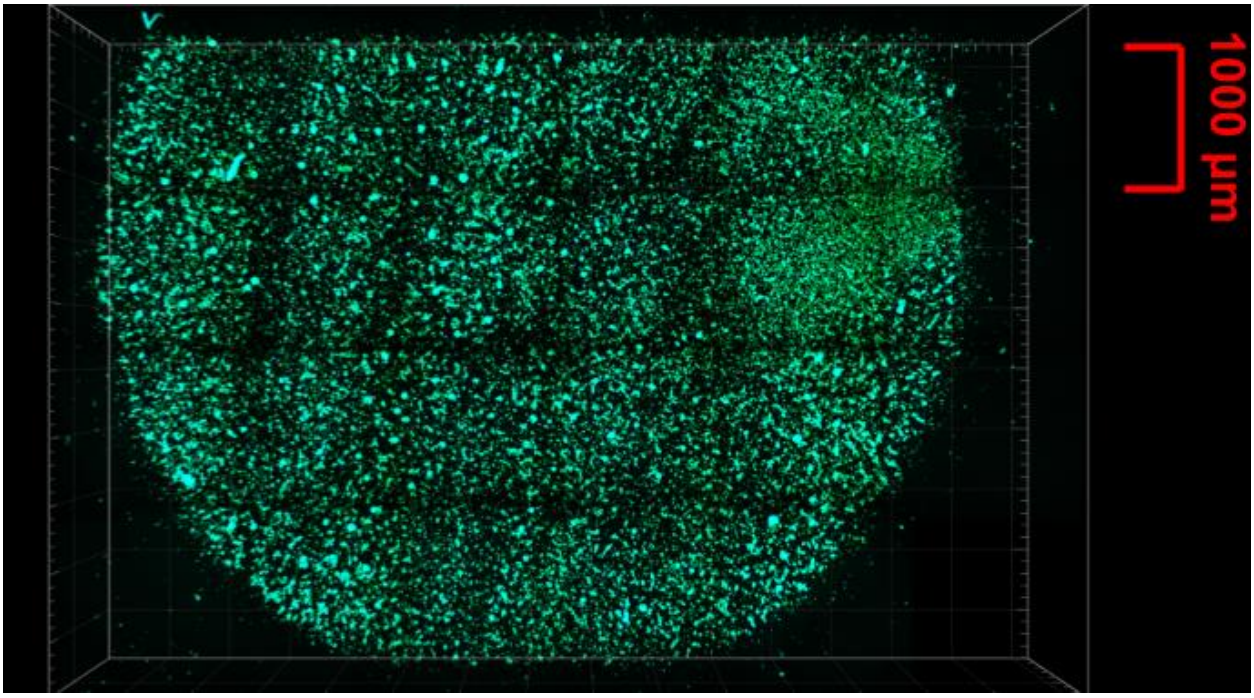

Figure 7: *A mosaic image of a 40 µm scaffold seeded with clone O MSCs stained with CFSE and NucBlue™ at the 72 hour timepoint.*

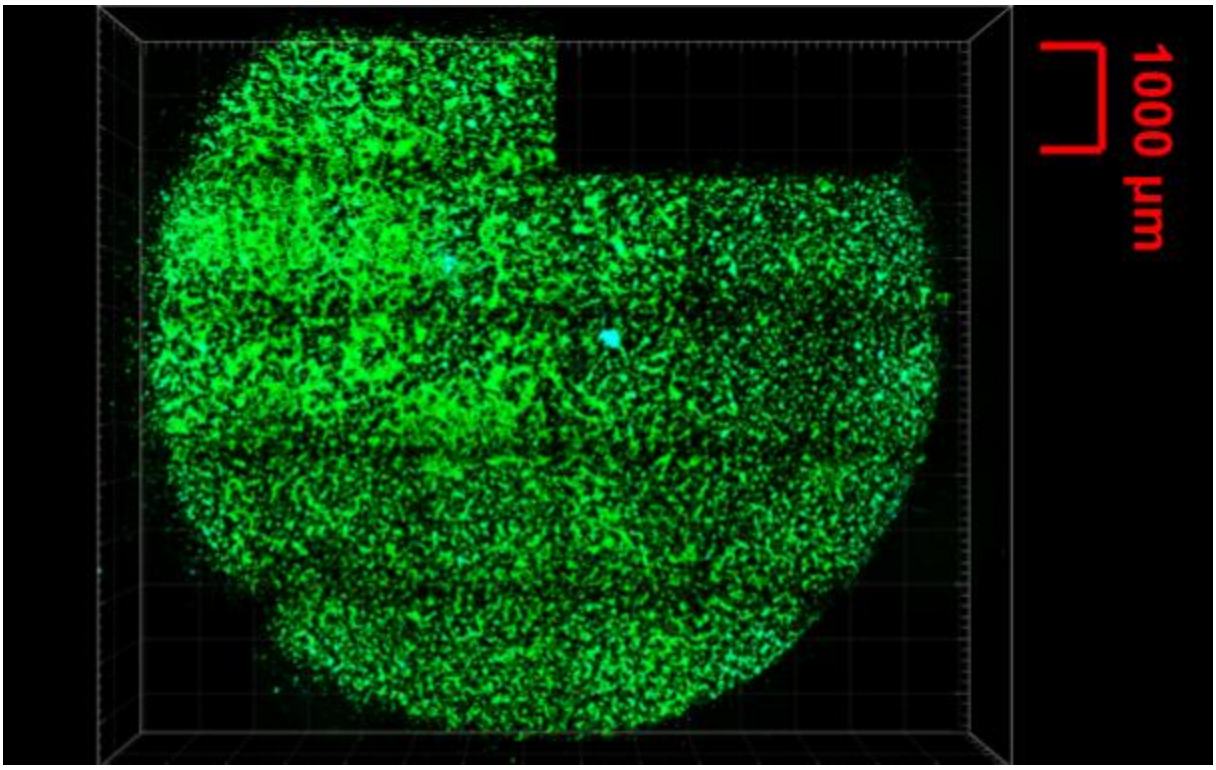

Figure 8: *A mosaic image of a 40 µm scaffold seeded with clone O MSCs stained with CFSE and NucBlue™ at the 96 hour timepoint.*

In addition to the MSCs exhibiting growth over the 96 hour time period, the cells formed three-dimensional pore-spanning connections over time [**Figure 9**]. At the 0 and 24 hour timepoints, we see the cells in the scaffold without making contact with each other. However, after 48 hours we see the cells connect and physically interact. The number of connections increases at the 72 and 96 hour timepoints. This suggests that prolonged growth within the scaffolds facilitates more complex three-dimensional interactions between the MSCs.

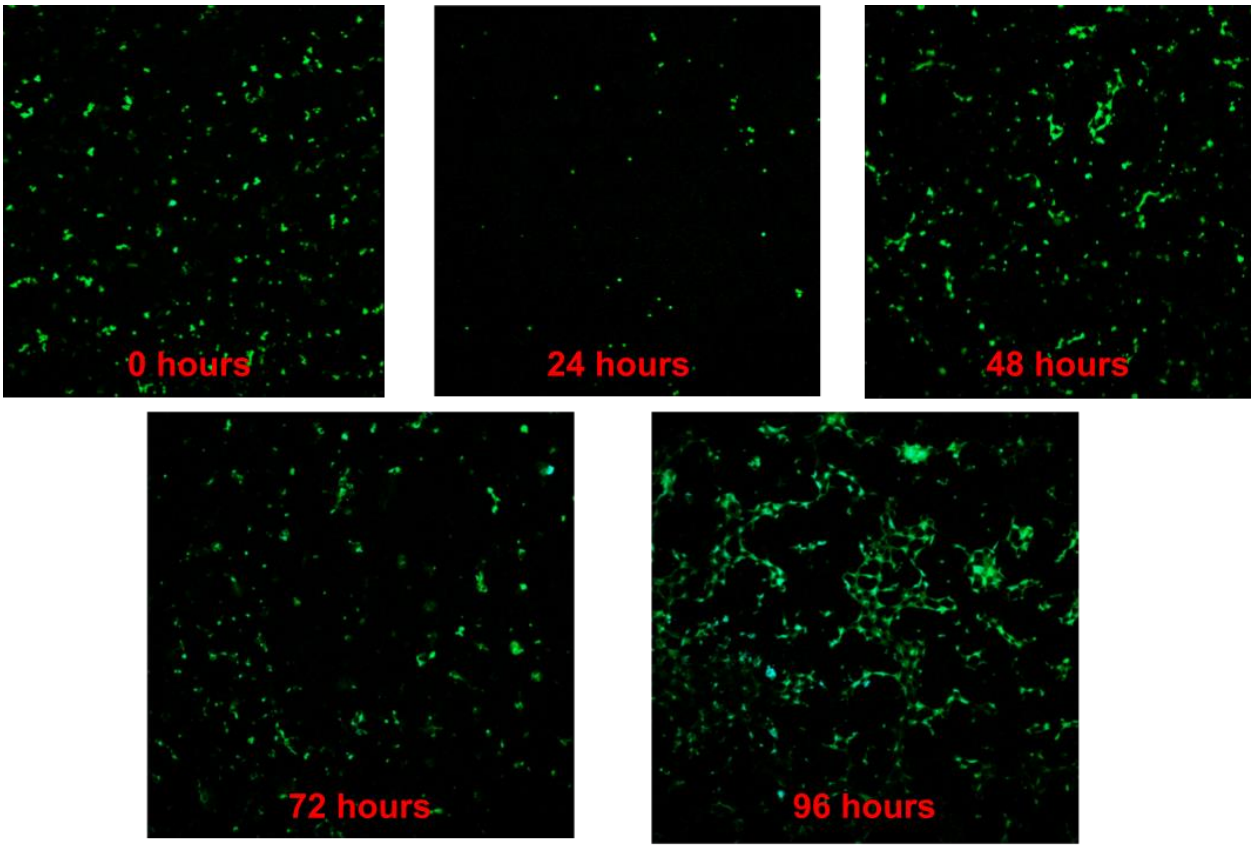

Figure 9: *Representative slices of the imaged PTS MSC cultures at 0, 24, 48, 72, and 96 hour timepoints. The images highlight the formation of three-dimensional connections between MSCs over time, supporting that MSCs are able to proliferate and form pore-spanning interactions within PTS cultures.*

When processed with ImageJ, the fluorescence of the MSCs was quantified and summarized in Table 3. There is an initial loss of cells as the MSCs leach into the medium, as seen in the decrease in CFSE fluorescence between the 0 and 24 hour timepoints. After the initial loss, sustained cell growth is observed in increased CFSE fluorescence between the 24 to 48, 48 to 72, and 72 to 96 hour timepoints. When comparing NucBlue™ fluorescence to CFSE fluorescence, the ratio initially increases between the 0 to 24 and 24 to 48 hour timepoints. This suggests that relative intensity of CFSE decreases as the dye is diluted when the MSCs divide and proliferate. However, this trend is reversed as the ratio of NucBlue™ fluorescence to CFSE fluorescence

decreases between the 48 to 72 and 72 to 96 hour timepoints. This may be due to NucBlue™ having to be administered to cells after growth and at the higher timepoints, the increased concentration and three-dimensional connections of the MSCs may prevent the penetration of the dye throughout the entire scaffold.

	0 Hours	**24 Hours**	**48 Hours**	**72 Hours**	**96 Hours**
Volume (mm^3)	24.8744	26.4744	24.8744	40.90376	44.50376
CFSE Fluorescence per Volume ($1/mm^3$)	1.885×10^8	2.282×10^7	4.414×10^7	3.203×10^8	9.104×10^8
NucBlue™ Fluorescence per Volume ($1/mm^3$)	1.146×10^6	1.039×10^6	9.710×10^6	8.109×10^4	1.444×10^6
NucBlue™ to CFSE Fluorescence Ratio	0.0053	0.0455	0.2200	0.0025	0.0016

Table 3: *Statistics of the MSCs within the imaged scaffolds obtained via ImageJ[60]. Fluorescence of CFSE and NucBlue™ refers to the data intensity sum, as measured with ImageJ, in the channel corresponding to each dye. There is a decrease in CFSE fluorescence from the 0 to 24 hour timepoint, reflective of cells leaching out into the medium. After the 24 hours timepoint, there is consistent increase in CFSE fluorescence after each timepoint. The ratio of NucBlue™ to CFSE increased from 0 to 24 and 24 to 48 hours, reflective of the relative fluorescence of NucBlue™ increasing as the relative fluorescence of CFSE decreasing as the MSCs proliferated. However, this trend reversed between 48 to 72 and 72 to 96 hours as the ratio of NucBlue™ to CFSE fluorescence decreased.*

Since MSCs were observed to expand within PTS cultures, their viability as a three-dimensional culture platform was supported. With the potential of PTS MSC cultures established, additional experiments were conducted investigating the impact of these cultures on the resident cells.

3.2 Gene Expression of Mesenchymal Stem Cells Grown Two- and Three-Dimensionally

During qPCR analysis, it was discovered that the autoclaved purified water used as a blank was contaminated (albeit with lower detected expression than the samples). Consequently, the results are presented with a low level of confidence. With the low level of confidence in mind, a pattern emerges among three of the five genetic markers (IL-6, IL-10, and TGFβ1) that display consistent increased expression in three-dimensional cultures [**Figure 10.A**, **10.B**, and **10.D**]. For iNOS expression levels, clone O exhibited increased expression in the three-dimensional cultures while clone N exhibited increased iNOS expression in only the 100 μm pore size PTS culture while the two-dimensional and 40 μm pore size PTS cultures exhibited similarly low levels of iNOS expression [**Figure 10.C**]. In the final marker, VEGFA, clone O exhibited comparable low expression levels among all of the cultures while clone N exhibited higher expression level only in the two-dimensional culture [**Figure 10.E**].

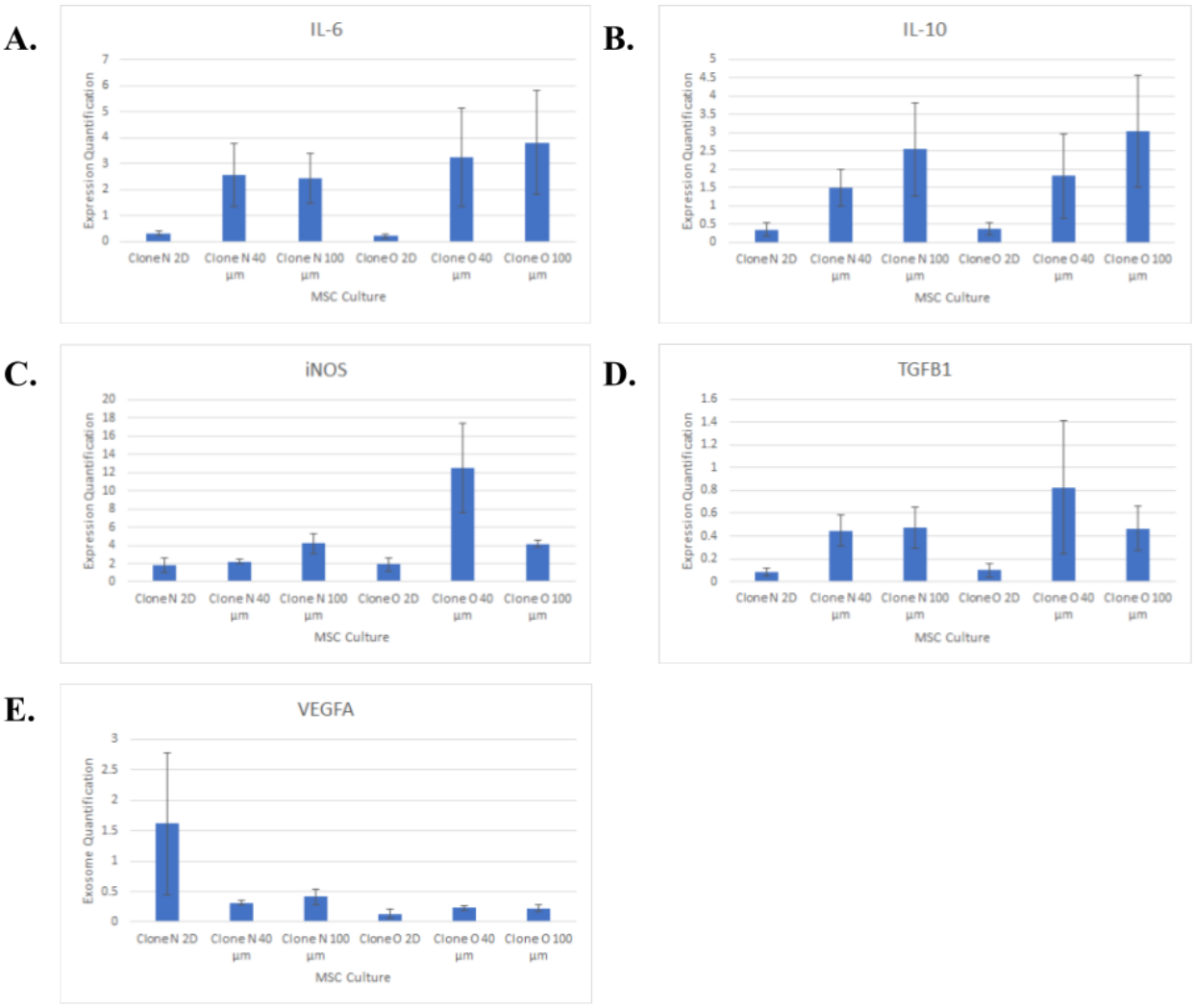

Figure 10: *Gene expression levels of IL-6, IL-10, iNOS, TGFβ1, VEGFA for MSCs cultured two- and three-dimensionally. The bar heights correspond to the average* $2^{-Av.\,\Delta Ct}$ *for each sample and probe while the error bars correspond to the standard error for the sample and probe.*

Despite the decreased level of confidence due to the contaminated blanks of the qPCR, the pattern of increased expression of MSCs within three-dimensional cultures is consistent enough to draw promising conclusions of potential increased effective capabilities of MSCs cultured three-dimensionally. Due to this pattern, additional investigations were conducted on MSCs

cultured two- and three-dimensionally when cocultured with RAW 264.7 cells at an increased timepoint.

3.3 Gene Expression Response of RAW 264.7 Cells Treated with Exosomes Generated from Mesenchymal Stem Cells in Two- and Three-Dimensional Cultures

The macrophage qPCR panel used can be divided into markers associated with M1- and M2-macrophage phenotypes. M1-macrophages are considered classically activated and are associated with a pro-inflammatory immune response[71]. Conversely, M2 macrophages are considered alternatively activated and are associated with wound healing and tissue repair.

As with the MSC qPCR, the water blanks used in this qPCR appeared contaminated (again with lower detected expression than the samples). Because of this, the results are presented with a low level of confidence. The RAW 264.7 cells treated with exosomes from the two-dimensionally cultured clone O MSCs exhibited significantly higher expression of every marker and were removed from the graphical representation as outliers. Regarding the expression of M2 associated genes, RAW 264.7 cells treated with exosomes from the two- and three-dimensionally cultured MSCs from either clone showed no statistical difference in expression levels for the seven genes analyzed[**Figure 11.A** and **11.B**]. There did not appear to be a dependency of M2 gene expression based on MSC clone, culture condition, or PTS pore size [**Figure 11.A** and **11.B**]. In fact, regardless of culture parameter, expression levels of each gene, save for TGFβ1,

were extremely low. This is indicative of no observable M2 polarization in RAW 264.7 cells treated with MSC exosomes from any culture conditions.

Regarding gene expression in M1-associated genes, CD86 and IL-6 were similarly upregulated in RAW 264.7 cells treated with exosomes from both clone O and N MSCs, regardless of culture conditions [**Figure 12**]. While upregulated, the expression levels of CD86 and IL-6 were relatively low. iNOS and IL1β expression levels were extremely low and showed no statistical dependency on clone type or culture condition.

A.

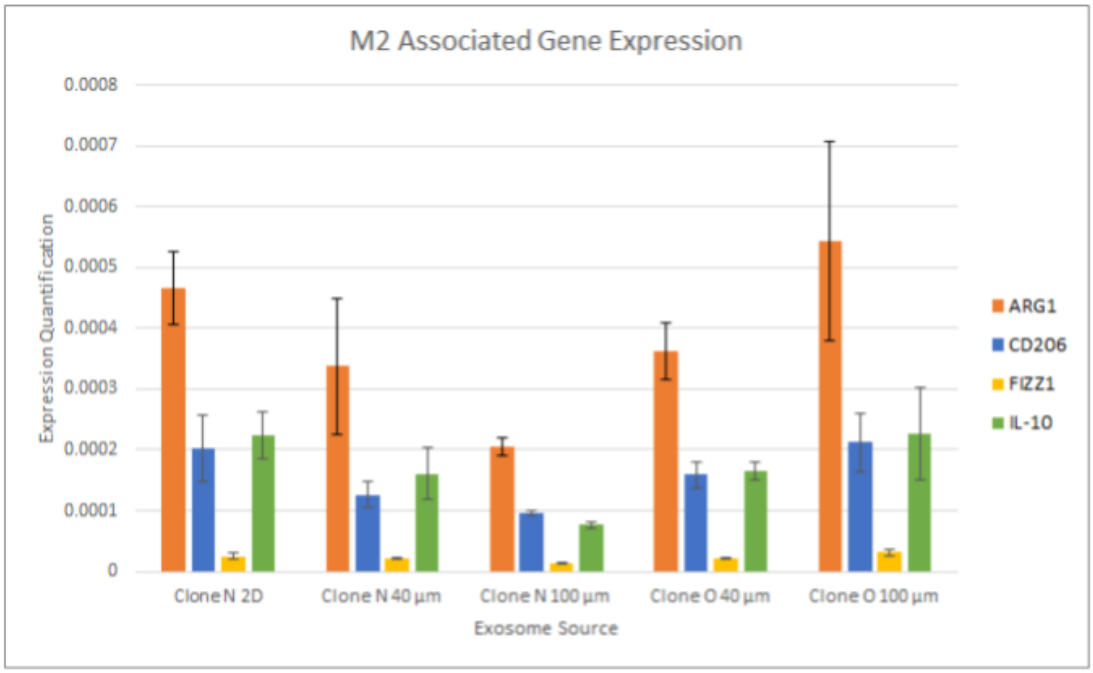

B.

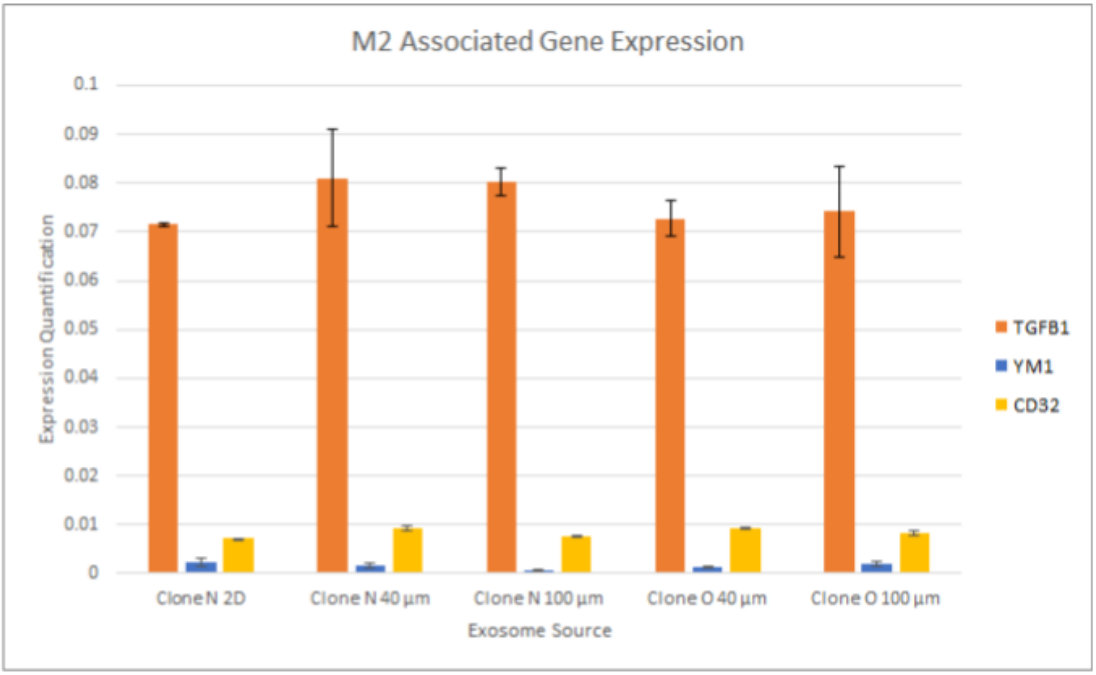

Figure 11: *Relative gene expression levels of the M2 macrophage phenotype associated genes. The bar heights correspond to the average* $2^{-Av.\ \Delta Ct}$ *for each sample and probe while the error bars correspond to the standard error for the sample and probe. The results are presented in two figures (**11.A** and **11.B**) to group the markers by relative expression levels and improve visibility.*

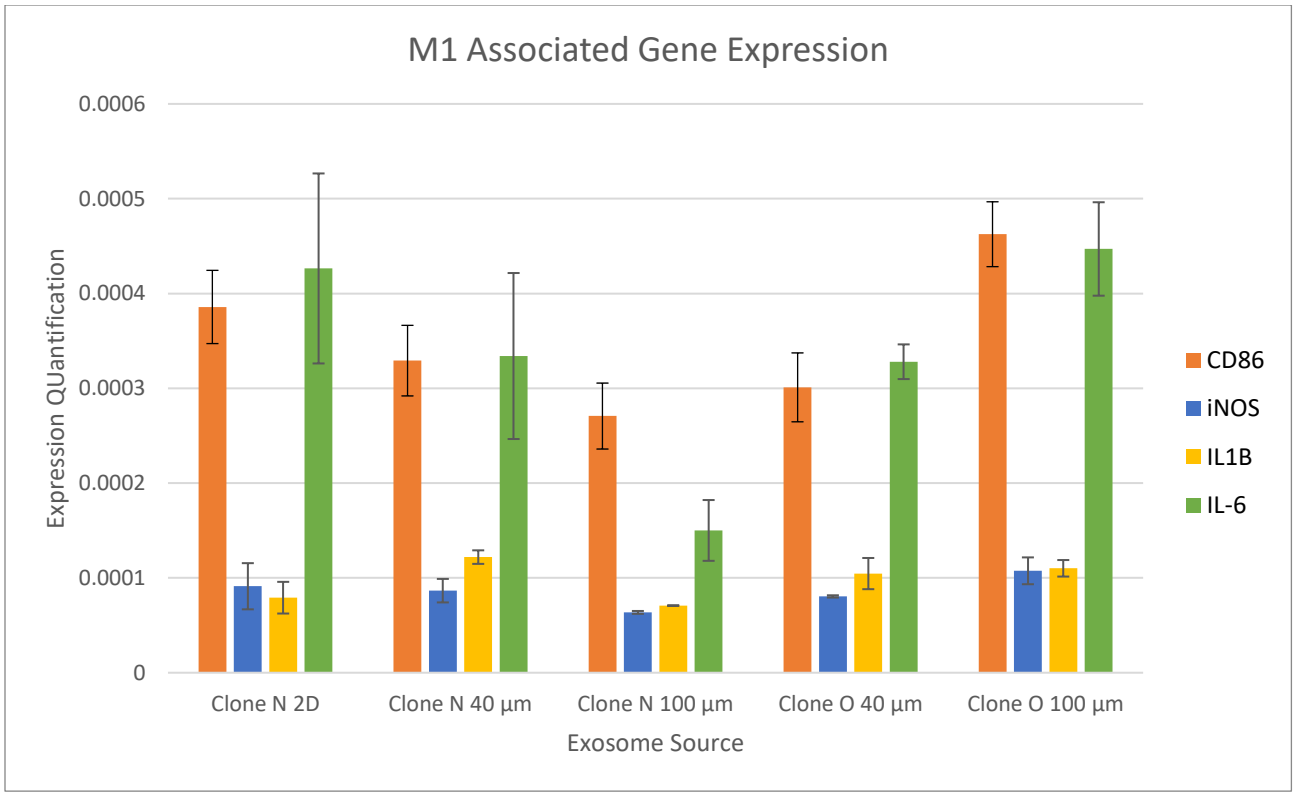

Figure 12: *Relative gene expression levels of the M1 macrophage phenotype associated genes in. The bar heights correspond to the average* $2^{-Av.\ \Delta Ct}$ *for each sample and probe while the error bars correspond to the standard error for the sample and probe.*

Aside from a slight elevation in TGFβ1 expression, exosomes generated from either clone cultivated in two- or three-dimensional cultures had no effect on polarizing RAW 264.7 cells towards an M1 or M2 phenotype. Literature shows that RAW 264.7 cells can be polarized via a variety of applied stimuli, mostly soluble cytokines or innate immune TLR agonists, such as LPS. It is not conclusive here whether exogenously applied exosomes were assimilated by the RAW 264.7 cells or whether exosomes from MSC cultures may exert their influence via other healing pathways and not through macrophage polarization. Additionally, the influence of exosomes may also require simultaneous stimulus via soluble factors, something not accounted for in the experiments described above. In order to account for additional paracrine factors that

may be required for MSCs' immunomodulation, subsequent experiments were conducted in which RAW 264.7 cells were cocultured with MSCs.

3.4 Gene Expression of RAW 264.7 Cells and Mesenchymal Stem Cells Cocultured Two- and Three-Dimensionally

Due to the contamination of previous qPCRs, the autoclaved purified water utilized as a blank in the qPCR was further purified by exposure to UV light. Despite this additional step in purification, the blank controls continued to appear as non-blank. The results of these qPCRs are presented in consideration of this contamination.

Consistent with previous experiments, a pattern emerged in genetic expression of the MSCs in which overall consistent increased expression of the majority of the genetic markers was observed in three-dimensional cultures [**Figure 13**]. In IL-6, IL-10 and iNOS expression, increased relative expression was observed among cells cultured three-dimensionally [**Figures 13.A-C**]. In TGFβ1 and VEGFA expression, expression levels were comparable between two- and three-dimensionally cultured cells with both MSC clones [**Figures 13.D-E**]. This supports the conclusions described above that PTS culture of MSCs may increase relative expression of genes associated with MSC paracrine effects.

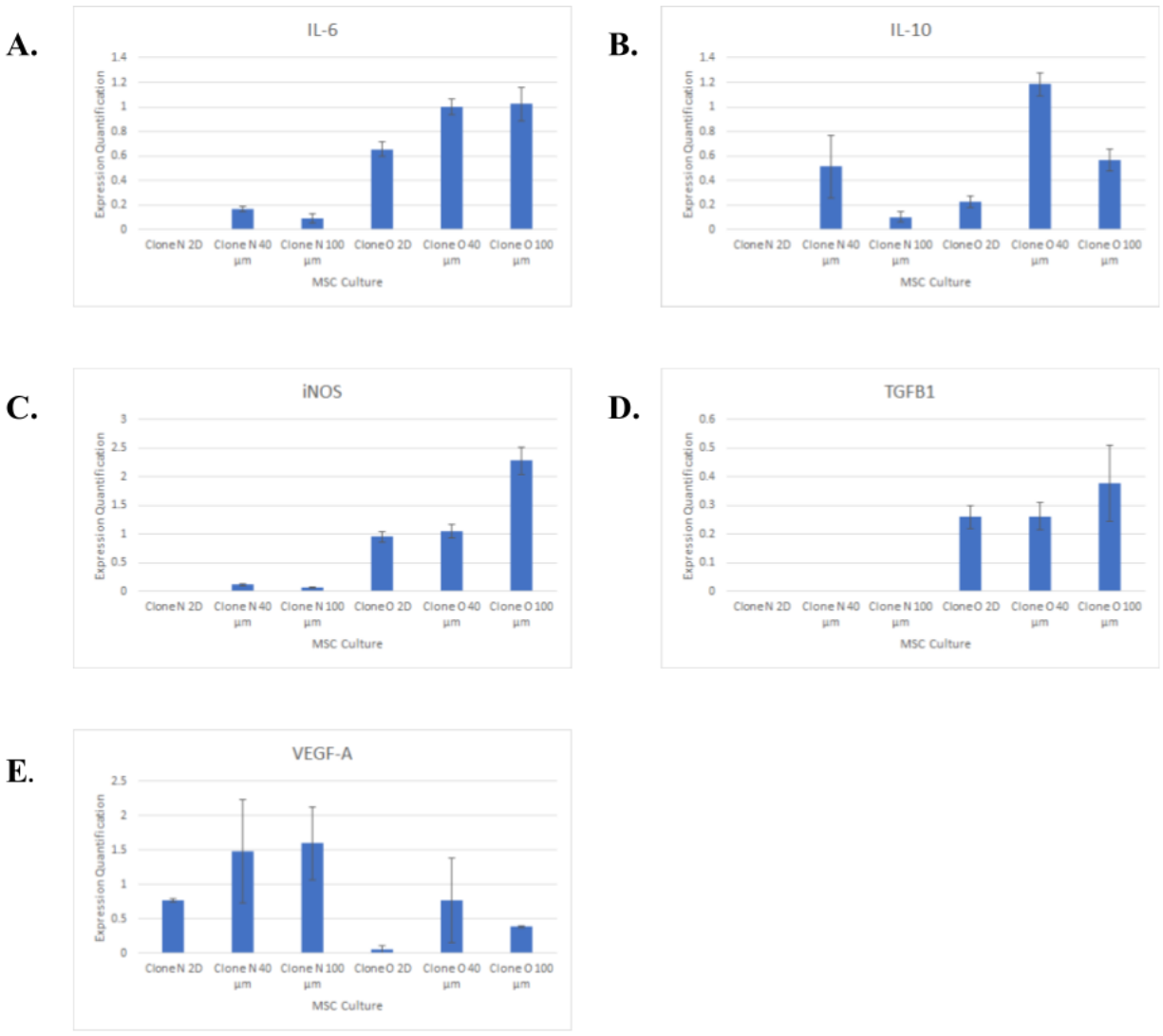

Figure 13: *Graphical representation of the expression levels of IL-6, IL-10, iNOS, TGFβ1, VEGFA. The bar heights correspond to the average* $2^{-Av.\ \Delta Ct}$ *for each sample and probe while the error bars correspond to the standard error for the sample and probe.*

While the MSCs in the cocultures exhibited differential relative expression based on culture conditions, no effect on RAW 264.7 polarization was observed regardless of MSC clone type or culture condition. Regarding the expression of M2-associated genes, overall low expression was observed for every genetic marker [**Figure 14**]. Some differences were observed between culture

conditions, for example, the RAW 264.7 cells cocultured with clone N MSCs in 40 μm PTS exhibited increased ARG1 expression compared to those cocultured with clone N MSCs in different culture conditions [**Figure 14.A**]. However, no clear pattern was established in these differential expression levels.

As with the M2-associated genes, no RAW 264.7 polarization was observed regarding the expression levels of M1-associated genes [**Figure 15**]. Similar to previous experiments, overall expression of all M1-associated genes was low and there was no statistically significant difference in expression level based on MSC clone type or culture condition.

A.

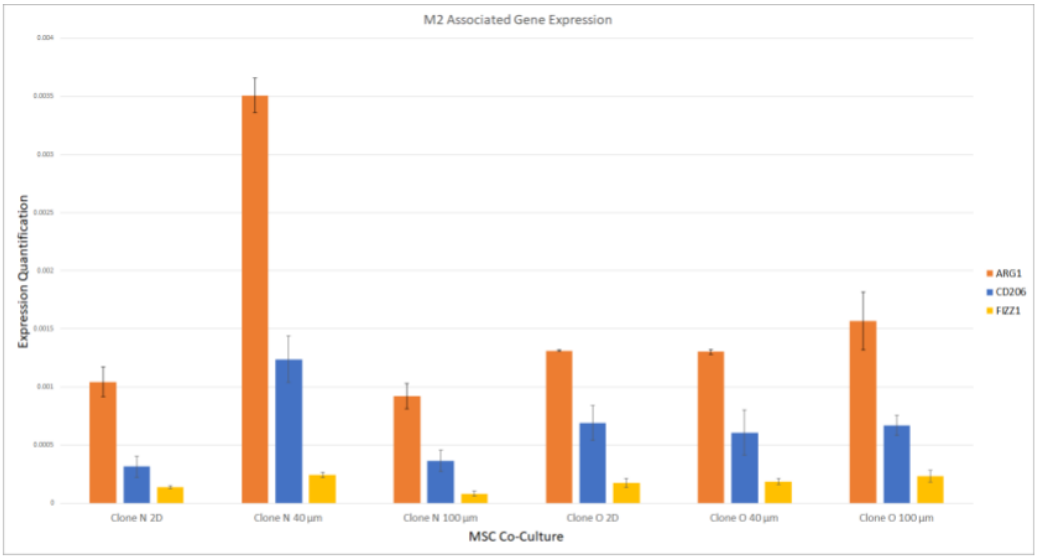

B.

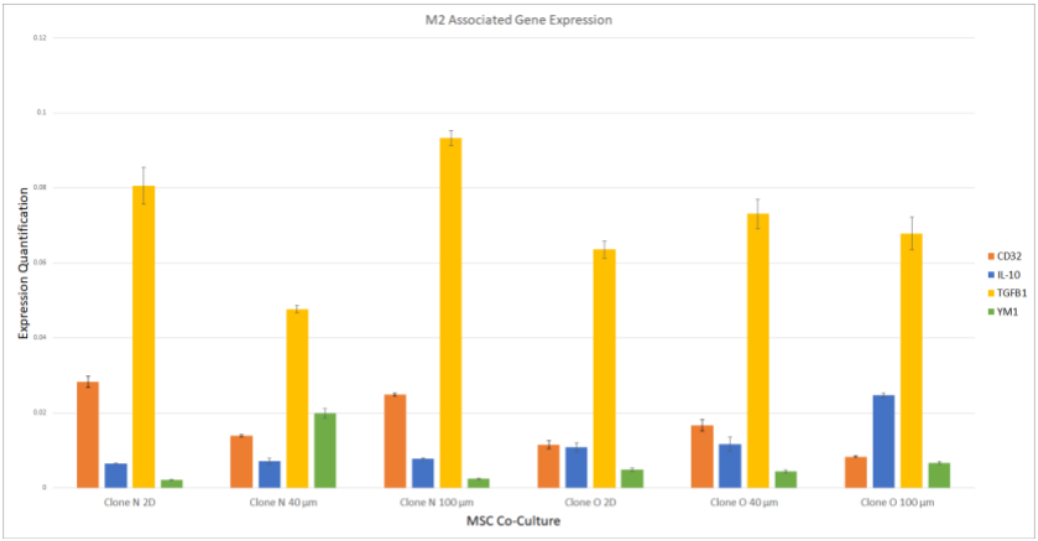

Figure 14: *Graphical representation of levels of the M2 macrophage associated genes in the macrophage panels. The bar heights correspond to the average* $2^{-Av.\ \Delta Ct}$ *for each sample and probe while the error bars correspond to the standard error for the sample and probe. The results are presented in two figures (**14.A** and **14.B**) to group the markers by relative expression levels and improve visibility.*

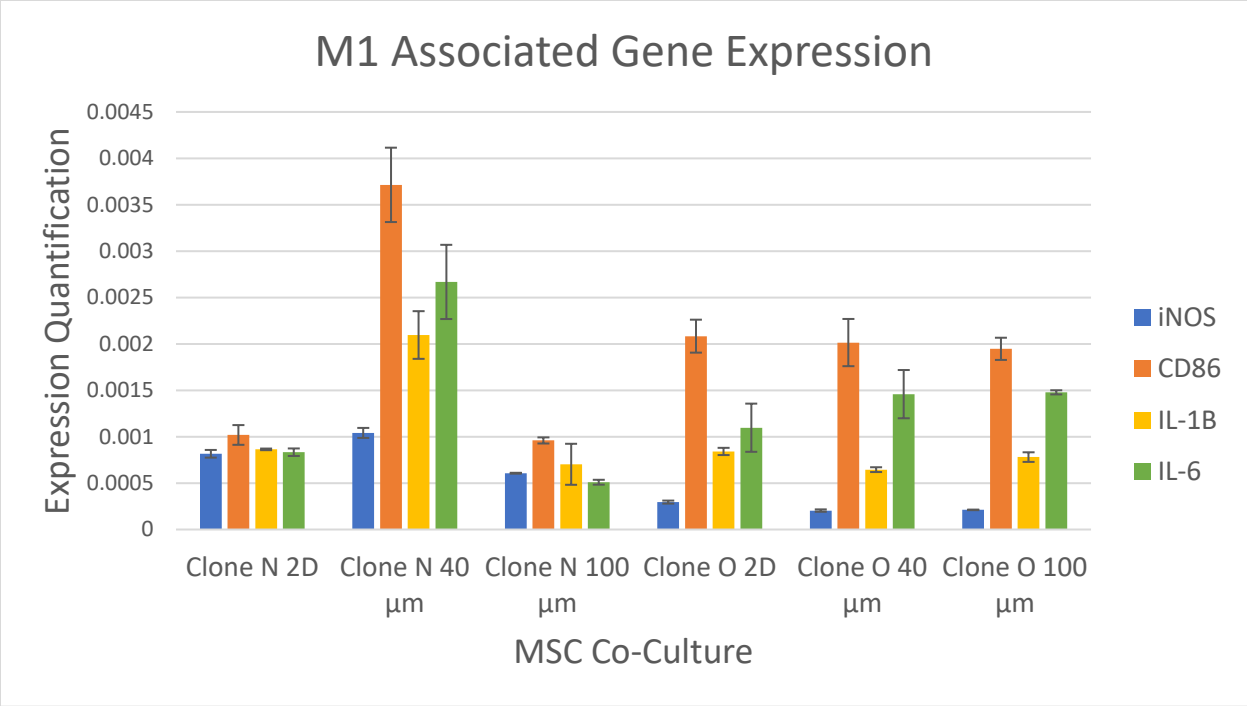

Figure 15: *Graphical representation of levels of the M1 macrophage associated genes in the macrophage panels. The bar heights correspond to the average* $2^{-Av.\,\Delta Ct}$ *for each sample and probe while the error bars correspond to the standard error for the sample and probe.*

The findings suggest that at this scale, regardless of the presence of soluble factors in addition to exosomes, MSCs without stimuli are incapable of polarizing RAW 264.7 cells via paracrine effects. This may be due to the lack of stimulus administered to the MSCs and RAW 264.7 cells or due to the relatively low number of cells utilized in these experiments, as MSCs have been observed to polarize RAW 264.7 cells when cultured in larger numbers. Future experiments could address these concerns by coculturing two- and three-dimensionally MSCs and RAW 264.7 cells at higher concentrations or with additional stimuli such as LPS.

CHAPTER 4. CONCLUSION

To conclude, PTS scaffolds present as a promising three-dimensional culture platform for MSCs but require additionally characterization for their impact on MSCs and their exosomes. MSCs were observed to expand and form connections within the PTS scaffold cultures, supporting their use for three-dimensional culture moving forward. When assessing the impact of three-dimensional culture on MSCs, overall increased expression was observed relative to traditional two-dimensional culture but these findings are undercut by a lowered level of confidence. Additionally, no strong pattern was observed in the varying effect of exosomes and other soluble paracrine factors derived from two- and three-dimensionally cultured MSCs when exposed to RAW 264.7 cells as well as the effect of coculturing RAW 264.7 cells with two- and three-dimensionally cultured MSCs. With these findings, there is enough promise in PTS-based culture of MSCs for further investigations. Additional work could be done by stimulating the MSCs within culture to elicit more immunomodulatory phenotypes, such as by treating the MSCs with Poly(I:C) to stimulate TLR3 expression. Another aspect of three-dimensional culture that could be investigated is the impact of PTS scaffold culture on the differentiation potential of MSCs, both by analyzing markers associated with stemness with sustained expansion as well as by analyzing differentiation when treating the cells with osteogenesis or adipogenesis differentiation medium. With the groundwork for PTS MSC culture laid in this project, we believe it can be further investigated and optimized for improved therapeutic potential of *in vitro* MSCs and their exosomes.

REFERENCES

1. Mushahary D, Spittler A, Kasper C, Weber V, Charwat V. Isolation, cultivation, and characterization of human mesenchymal stem cells. Cytometry A. 2018;93(1):19-31.

2. Han Y, Li X, Zhang Y, Chang F, Ding J. Mesenchymal Stem Cells for Regenerative Medicine. Cells. 2019;8(8).

3. Xu L, Liu Y, Sun Y, et al. Tissue source determines the differentiation potentials of mesenchymal stem cells: a comparative study of human mesenchymal stem cells from bone marrow and adipose tissue. Stem Cell Res Ther. 2017;8(1):275.

4. Cornelissen AS, Maijenburg MW, Nolte MA, Voermans C. Organ-specific migration of mesenchymal stromal cells: Who, when, where and why? Immunol Lett. 2015;168(2):159-169.

5. Phinney DG, Pittenger MF. Concise Review: MSC-Derived Exosomes for Cell-Free Therapy. Stem Cells. 2017;35(4):851-858.

6. English K, Ryan JM, Tobin L, Murphy MJ, Barry FP, Mahon BP. Cell contact, prostaglandin E(2) and transforming growth factor beta 1 play non-redundant roles in human mesenchymal stem cell induction of CD4+CD25(High) forkhead box P3+ regulatory T cells. Clin Exp Immunol. 2009;156(1):149-160.

7. Ren G, Zhao X, Zhang L, et al. Inflammatory cytokine-induced intercellular adhesion molecule-1 and vascular cell adhesion molecule-1 in mesenchymal stem cells are critical for immunosuppression. J Immunol. 2010;184(5):2321-2328.

8. Corcione A, Benvenuto F, Ferretti E, et al. Human mesenchymal stem cells modulate B-cell functions. Blood. 2006;107(1):367-372.

9. Gao F, Chiu SM, Motan DA, et al. Mesenchymal stem cells and immunomodulation: current status and future prospects. Cell Death Dis. 2016;7:e2062.

10. Lin PP, Wang Y, Lozano G. Mesenchymal Stem Cells and the Origin of Ewing's Sarcoma. Sarcoma. 2011;2011.

11. Amariglio N, Hirshberg A, Scheithauer BW, et al. Donor-derived brain tumor following neural stem cell transplantation in an ataxia telangiectasia patient. PLoS Med. 2009;6(2):e1000029.

12. Karnoub AE, Dash AB, Vo AP, et al. Mesenchymal stem cells within tumour stroma promote breast cancer metastasis. Nature. 2007;449(7162):557-563.

13. Li W, Ren G, Huang Y, et al. Mesenchymal stem cells: a double-edged sword in regulating immune responses. Cell Death Differ. 2012;19(9):1505-1513.

14. Popova AP, Bozyk PD, Goldsmith AM, et al. Autocrine production of TGF-beta1 promotes myofibroblastic differentiation of neonatal lung mesenchymal stem cells. Am J Physiol Lung Cell Mol Physiol. 2010;298(6):L735-743.

15. Kalluri R, LeBleu VS. The biology, function, and biomedical applications of exosomes. Science. 2020;367(6478).

16. Marote A, Teixeira FG, Mendes-Pinheiro B, Salgado AJ. MSCs-Derived Exosomes: Cell-Secreted Nanovesicles with Regenerative Potential. Front Pharmacol. 2016;7:231.

17. Lin J, Li J, Huang B, et al. Exosomes: novel biomarkers for clinical diagnosis. ScientificWorldJournal. 2015;2015:657086.

18. Graner MW, Alzate O, Dechkovskaia AM, et al. Proteomic and immunologic analyses of brain tumor exosomes. FASEB J. 2009;23(5):1541-1557.

19. Lv LL, Cao YH, Ni HF, et al. MicroRNA-29c in urinary exosome/microvesicle as a biomarker of renal fibrosis. Am J Physiol Renal Physiol. 2013;305(8):F1220-1227.
20. Wortzel I, Dror S, Kenific CM, Lyden D. Exosome-Mediated Metastasis: Communication from a Distance. Dev Cell. 2019;49(3):347-360.
21. Takahashi A, Okada R, Nagao K, et al. Exosomes maintain cellular homeostasis by excreting harmful DNA from cells. Nat Commun. 2017;8:15287.
22. Raimondo S, Saieva L, Corrado C, et al. Chronic myeloid leukemia-derived exosomes promote tumor growth through an autocrine mechanism. Cell Commun Signal. 2015;13:8.
23. Demory Beckler M, Higginbotham JN, Franklin JL, et al. Proteomic analysis of exosomes from mutant KRAS colon cancer cells identifies intercellular transfer of mutant KRAS. Mol Cell Proteomics. 2013;12(2):343-355.
24. Pavlyukov MS, Yu H, Bastola S, et al. Apoptotic Cell-Derived Extracellular Vesicles Promote Malignancy of Glioblastoma Via Intercellular Transfer of Splicing Factors. Cancer Cell. 2018;34(1):119-135.e110.
25. Tian T, Zhang HX, He CP, et al. Surface functionalized exosomes as targeted drug delivery vehicles for cerebral ischemia therapy. Biomaterials. 2018;150:137-149.
26. Li SP, Lin ZX, Jiang XY, Yu XY. Exosomal cargo-loading and synthetic exosome-mimics as potential therapeutic tools. Acta Pharmacol Sin. 2018;39(4):542-551.
27. Katakowski M, Buller B, Zheng X, et al. Exosomes from marrow stromal cells expressing miR-146b inhibit glioma growth. Cancer Lett. 2013;335(1):201-204.
28. Salunkhe S, Dheeraj, Basak M, Chitkara D, Mittal A. Surface functionalization of exosomes for target-specific delivery and in vivo imaging & tracking: Strategies and significance. J Control Release. 2020;326:599-614.
29. Mendt M, Rezvani K, Shpall E. Mesenchymal stem cell-derived exosomes for clinical use. Bone Marrow Transplant. 2019;54(Suppl 2):789-792.
30. Willis GR, Fernandez-Gonzalez A, Anastas J, et al. Mesenchymal Stromal Cell Exosomes Ameliorate Experimental Bronchopulmonary Dysplasia and Restore Lung Function through Macrophage Immunomodulation. Am J Respir Crit Care Med. 2018;197(1):104-116.
31. Cosenza S, Toupet K, Maumus M, et al. Mesenchymal stem cells-derived exosomes are more immunosuppressive than microparticles in inflammatory arthritis. Theranostics. 2018;8(5):1399-1410.
32. Watanabe T, Hoshikawa Y, Ishibashi N, et al. Mesenchymal stem cells attenuate ischemia-reperfusion injury after prolonged cold ischemia in a mouse model of lung transplantation: a preliminary study. Surg Today. 2017;47(4):425-431.
33. Tomasoni S, Longaretti L, Rota C, et al. Transfer of growth factor receptor mRNA via exosomes unravels the regenerative effect of mesenchymal stem cells. Stem Cells Dev. 2013;22(5):772-780.
34. He J, Wang Y, Sun S, et al. Bone marrow stem cells-derived microvesicles protect against renal injury in the mouse remnant kidney model. Nephrology (Carlton). 2012;17(5):493-500.
35. Elahi FM, Farwell DG, Nolta JA, Anderson JD. Preclinical translation of exosomes derived from mesenchymal stem/stromal cells. Stem Cells. 2020;38(1):15-21.
36. Uder C, Brückner S, Winkler S, Tautenhahn HM, Christ B. Mammalian MSC from selected species: Features and applications. Cytometry A. 2018;93(1):32-49.

37. Rashedi I, Talele N, Wang XH, Hinz B, Radisic M, Keating A. Collagen scaffold enhances the regenerative properties of mesenchymal stromal cells. PLoS One. 2017;12(10):e0187348.
38. Miceli V, Pampalone M, Vella S, Carreca AP, Amico G, Conaldi PG. Comparison of Immunosuppressive and Angiogenic Properties of Human Amnion-Derived Mesenchymal Stem Cells between 2D and 3D Culture Systems. Stem Cells Int. 2019;2019:7486279.
39. Cheng NC, Wang S, Young TH. The influence of spheroid formation of human adipose-derived stem cells on chitosan films on stemness and differentiation capabilities. Biomaterials. 2012;33(6):1748-1758.
40. Naito H, Yoshimura M, Mizuno T, Takasawa S, Tojo T, Taniguchi S. The advantages of three-dimensional culture in a collagen hydrogel for stem cell differentiation. J Biomed Mater Res A. 2013;101(10):2838-2845.
41. Rashid S, Qazi RE, Malick TS, et al. Effect of valproic acid on the hepatic differentiation of mesenchymal stem cells in 2D and 3D microenvironments. Mol Cell Biochem. 2021;476(2):909-919.
42. Yu SJ, Choi G, Cho Y, et al. Three-Dimensional Spheroid Culture on Polymer-Coated Surface Potentiate Stem Cell Functions via Enhanced Cell-Extracellular Matrix Interactions. ACS Biomater Sci Eng. 2020;6(4):2240-2250.
43. Ryu NE, Lee SH, Park H. Spheroid Culture System Methods and Applications for Mesenchymal Stem Cells. Cells. 2019;8(12).
44. McKee C, Chaudhry GR. Advances and challenges in stem cell culture. Colloids Surf B Biointerfaces. 2017;159:62-77.
45. Ravi M, Paramesh V, Kaviya SR, Anuradha E, Solomon FD. 3D cell culture systems: advantages and applications. J Cell Physiol. 2015;230(1):16-26.
46. Prasopthum A, Cooper M, Shakesheff KM, Yang J. Three-Dimensional Printed Scaffolds with Controlled Micro-/Nanoporous Surface Topography Direct Chondrogenic and Osteogenic Differentiation of Mesenchymal Stem Cells. ACS Appl Mater Interfaces. 2019;11(21):18896-18906.
47. Qazi TH, Tytgat L, Dubruel P, Duda GN, Van Vlierberghe S, Geissler S. Extrusion Printed Scaffolds with Varying Pore Size As Modulators of MSC Angiogenic Paracrine Effects. ACS Biomater Sci Eng. 2019;5(10):5348-5358.
48. Kinneberg KR, Nirmalanandhan VS, Juncosa-Melvin N, et al. Chondroitin-6-sulfate incorporation and mechanical stimulation increase MSC-collagen sponge construct stiffness. J Orthop Res. 2010;28(8):1092-1099.
49. Ratner B, Marshall A, Inventors; University of Washington, assignee. Novel Porous Biomaterials2008.
50. Bryers JD, Giachelli CM, Ratner BD. Engineering biomaterials to integrate and heal: the biocompatibility paradigm shifts. Biotechnol Bioeng. 2012;109(8):1898-1911.
51. Hady TF, Hwang B, Pusic AD, et al. Uniform 40-µm-pore diameter precision templated scaffolds promote a pro-healing host response by extracellular vesicle immune communication. J Tissue Eng Regen Med. 2021;15(1):24-36.
52. Marshall AJ, Ratner BD. Quantitative characterization of sphere-templated porous biomaterials. AIChE Journal. 2005;51(4):1221-1232.

53. Madden LR, Mortisen DJ, Sussman EM, et al. Proangiogenic scaffolds as functional templates for cardiac tissue engineering. Proc Natl Acad Sci U S A. 2010;107(34):15211-15216.

54. Chen R, Ma H, Zhang L, Bryers JD. Precision-porous templated scaffolds of varying pore size drive dendritic cell activation. Biotechnol Bioeng. 2018;115(4):1086-1095.

55. Hwang B, Liles WC, Waworuntu R, Mulligan MS. Pretreatment with bone marrow-derived mesenchymal stromal cell-conditioned media confers pulmonary ischemic tolerance. J Thorac Cardiovasc Surg. 2016;151(3):841-849.

56. CellTrace™ Cell Proliferation Kits. https://www.thermofisher.com/document-connect/document-connect.html?url=https%3A%2F%2Fassets.thermofisher.com%2FTFS-Assets%2FLSG%2Fmanuals%2FMAN0002595_CellTrace_Cell_Proliferation_Kits_UG.pdf&title=VXNlciBHdWlkZTogQ2VsbFRyYWNlIENlbGwgUHJvbGlmZXJhdGlvbiBLaXRz.

57. NucBlue® Live ReadyProbes® Reagent Protocol. https://www.thermofisher.com/us/en/home/references/protocols/cell-and-tissue-analysis/protocols/nucblue-live-readyprobes-protocol.html.

58. Olympus FV1000 Confocal & Multiphoton Microscope. https://ecdoi.ecu.edu/ecdoi-core/olympus-fv1000-confocal-multiphoton-microscope/.

59. Emmenlauer M, Ronneberger O, Ponti A, et al. XuvTools: free, fast and reliable stitching of large 3D datasets. J Microsc. 2009;233(1):42-60.

60. Schneider CA, Rasband WS, Eliceiri KW. NIH Image to ImageJ: 25 years of image analysis. Nat Methods. 2012;9(7):671-675.

61. Corning™ Transwell™ Multiple Well Plate with Permeable Polyester Membrane Inserts. https://www.fishersci.com/shop/products/costar-transwell-clear-polyester-membrane-inserts-for-24-well-plates-4/07200170.

62. Dorronsoro A, Lang V, Ferrin I, et al. Intracellular role of IL-6 in mesenchymal stromal cell immunosuppression and proliferation. Sci Rep. 2020;10(1):21853.

63. Wang J, Ren H, Yuan X, Ma H, Shi X, Ding Y. Interleukin-10 secreted by mesenchymal stem cells attenuates acute liver failure through inhibiting pyroptosis. Hepatol Res. 2018;48(3):E194-E202.

64. Kyurkchiev D, Bochev I, Ivanova-Todorova E, et al. Secretion of immunoregulatory cytokines by mesenchymal stem cells. World J Stem Cells. 2014;6(5):552-570.

65. Sonar SA, Lal G. The iNOS Activity During an Immune Response Controls the CNS Pathology in Experimental Autoimmune Encephalomyelitis. Front Immunol. 2019;10:710.

66. Maria ATJ, Rozier P, Fonteneau G, et al. iNOS Activity Is Required for the Therapeutic Effect of Mesenchymal Stem Cells in Experimental Systemic Sclerosis. Front Immunol. 2018;9:3056.

67. Liu F, Qiu H, Xue M, et al. MSC-secreted TGF-β regulates lipopolysaccharide-stimulated macrophage M2-like polarization via the Akt/FoxO1 pathway. Stem Cell Res Ther. 2019;10(1):345.

68. Putra A, Alif I, Hamra N, et al. MSC-released TGF-β regulate α-SMA expression of myofibroblast during wound healing. J Stem Cells Regen Med. 2020;16(2):73-79.

69. Ge Q, Zhang H, Hou J, et al. VEGF secreted by mesenchymal stem cells mediates the differentiation of endothelial progenitor cells into endothelial cells via paracrine mechanisms. Mol Med Rep. 2018;17(1):1667-1675.
70. An Y, Liu WJ, Xue P, et al. Autophagy promotes MSC-mediated vascularization in cutaneous wound healing via regulation of VEGF secretion. Cell Death Dis. 2018;9(2):58.
71. Atri C, Guerfali FZ, Laouini D. Role of Human Macrophage Polarization in Inflammation during Infectious Diseases. Int J Mol Sci. 2018;19(6).